

This work was written as part of one of the author's official duties as an Employee of the United States Government and is therefore a work of the United States Government. In accordance with 17 U.S.C. 105, no copyright protection is available for such works under U.S. Law.

Public Domain Mark 1.0

<https://creativecommons.org/publicdomain/mark/1.0/>

Access to this work was provided by the University of Maryland, Baltimore County (UMBC) ScholarWorks@UMBC digital repository on the Maryland Shared Open Access (MD-SOAR) platform.

Please provide feedback

Please support the ScholarWorks@UMBC repository by emailing scholarworks-group@umbc.edu and telling us what having access to this work means to you and why it's important to you. Thank you.

Satellite estimation of spectral surface UV irradiance

2. Effects of homogeneous clouds and snow

N. A. Krotkov,^{1,2} J. R. Herman,² P. K. Bhartia,² V. Fioletov,³ and Z. Ahmad^{4,2}

Abstract. This paper extends the theoretical analysis of the estimation of the surface UV irradiance from satellite ozone and reflectivity data from a clear-sky case to a cloudy atmosphere and snow-covered surface. Two methods are compared for the estimation of cloud-transmission factor C_T , the ratio of cloudy to clear-sky surface irradiance: (1) the Lambert equivalent reflectivity (LER) method and (2) a method based on radiative transfer calculations for a homogeneous (plane parallel) cloud embedded into a molecular atmosphere with ozone absorption. The satellite-derived C_T from the NASA Total Ozone Mapping Spectrometer (TOMS) is compared with ground-based C_T estimations from the Canadian network of Brewer spectrometers for the period 1989–1998. For snow-free conditions the TOMS derived C_T at 324 nm approximately agrees with Brewer data with a correlation coefficient of ~ 0.9 and a standard deviation of ~ 0.1 . The key source of uncertainty is the different size of the TOMS FOV (~ 100 km field of view) and the much smaller ground instrument FOV. As expected, the standard deviations of weekly and monthly C_T averages were smaller than for daily values. The plane-parallel cloud method produces a systematic C_T bias relative to the Brewer data ($+7\%$ at low solar zenith angles to -10% at large solar zenith angles). The TOMS algorithm can properly account for conservatively scattering clouds and snow/ice if the regional snow albedo R_s is known from outside data. Since R_s varies on a daily basis, using a climatology will result in additional error in the satellite-estimated C_T . The C_T error has the same sign as the R_s error and increases over highly reflecting surfaces. Finally, clouds polluted with absorbing aerosols transmit less radiation to the ground than conservative clouds for the same satellite reflectance and flatten spectral dependence of C_T . Both effects reduce C_T compared to that estimated assuming conservative cloud scattering. The error increases if polluted clouds are over snow.

1. Introduction

The main reason for estimating UV (280–400 nm) irradiance at the Earth's surface concerns human health and related biological issues for plants and animals, as well as issues of air quality and UV damage to materials. Since photons in the UV-B range (280–320 nm) have sufficient energy to cause breaking of bonds in DNA molecules, any increase over long-term customary amounts is a cause for considerable concern. For this purpose the quantities of main interest are the maximum amounts of UV irradiance at a location during a given season and the cumulative exposure to this radiation over periods from days to months. In the absence of snow, clouds, and aerosols the UV exposure can be calculated accurately in a Rayleigh-scattering atmosphere using total ozone and ground reflectivity measurements from either ground-based or satellite instruments.

Madronich [1992] has first calculated changes in biologically active UV irradiance from 1979 to 1989 in clear-sky and aero-

sol-free conditions on a global scale using extraterrestrial solar irradiance measurements and satellite ozone data from the NASA Total Ozone Mapping Spectrometer (TOMS) as inputs to a fast delta-Eddington radiative transfer code. Zonal average changes in UV irradiance, including the effects of clouds and nonabsorbing aerosols, were estimated for the entire Nimbus-7 TOMS data record (1979–1992) by Herman *et al.* [1996]. Satellite estimation of the effect of increasing UV-B due to decreasing total ozone has been confirmed by many ground-based UV-B measurements at different locations (for most recent update, see WMO [1999]). It was also recognized that aerosol information is important to obtain agreement of clear-sky UV radiation models with ground-based UV measurements [Vogelmann *et al.*, 1992; Davies, 1993; Mayer *et al.*, 1997; Weihs and Webb, 1997; Kylling *et al.*, 1998]. Some models have also suggested that upward trends in tropospheric aerosol or tropospheric ozone may have locally modified UV-B trends caused by stratospheric ozone changes [Brühl and Crutzen, 1989; Liu *et al.*, 1991; Sabziparvar *et al.*, 1998]. TOMS UV reflectivity can be used to correct for absorbing aerosols at a known altitude by forming the aerosol index (AI), as discussed by Krotkov *et al.* [1998]. However, the AI technique does not have the sensitivity to detect weakly absorbing aerosols close to the ground which are often found in urban atmospheres [Dickerson *et al.*, 1997; Torres *et al.*, 1998; Jacobson, 1999; Herman *et al.*, 1999]. This problem has been addressed by using the TOMS radiances directly to calculate the aerosol optical depth and single-scattering albedo all the way to the surface [Torres *et al.*

¹Goddard Earth Sciences and Technology Center, University of Maryland at Baltimore County, Maryland.

²Laboratory for Atmospheres, NASA Goddard Space Flight Center, Greenbelt, Maryland.

³Meteorological Service of Canada, Downsview, Ontario, Canada.

⁴Science and Data Systems, Silver Spring, Maryland.

al., 1998]. To date, only the AI method has been applied, so the uncertainty in satellite-measured sources of tropospheric pollution remains a key source of error [Herman et al., 1999] in estimating surface UV for industrial regions. This paper addresses additional sources of error related to cloud and snow effects.

Several methods have been suggested to correct satellite-estimated clear-sky UV irradiance for the effect of cloudiness [Lubin et al., 1994; Eck et al., 1995; Lubin and Jensen, 1995; Meerkötter et al., 1997; Rublev et al., 1997; Lubin et al., 1998; Li et al., 2000; Matthijsen et al., 2000; Verdebout, 2000]. These include multi-instrument approaches or using UV reflectance channels of satellite ozone-measuring instruments. High-resolution (~ 1 km) visible reflectance data from the advanced very high resolution radiometer (AVHRR) instruments aboard NOAA weather polar orbiting satellites were used (in combination with external ozone data) to calculate UV maps for several geographical areas: Germany [Meerkötter et al., 1997], the Antarctic Peninsula [Lubin et al., 1994], and the Moscow region, Russia [Rublev et al., 1997]. Matthijsen et al. [2000] have used composite cloud data accumulated by the International Satellite Cloud Climatology Project (ISCCP) [Rossow and Schiffer, 1991] to estimate spatially averaged cloud reduction over Europe in 1993–1994. Verdebout [2000] have proposed to use both satellite (GOME, Meteosat) and ancillary data to generate surface UV maps over Europe with a spatial resolution of 0.05° and potentially on a half-hour basis. Another approach is to combine the TOMS ozone data with shortwave cloud reflectance measurements from the NASA Earth Radiation Budget Experiment (ERBE) [Lubin and Jensen, 1995; Lubin et al., 1998]. Since the cloud transmittance is spectrally dependent [Nack and Green, 1974; Seckmeyer et al., 1996; Krotkov et al., 1997; Frederick and Erlick, 1997; Kylling et al., 1998; Matthijsen et al., 2000] and can be modified by aerosols [Erlick et al., 1998], estimation of UV transmittance based on visible (i.e., AVHRR, geostationary satellites) or shortwave reflectance (i.e., ERBE) data is not straightforward. In addition, such methods are susceptible to other uncertainties (i.e., water vapor absorption).

A more direct approach is to use the UV reflectivity derived from the 360 or 380 nm channels of ozone-measuring instruments. The method has been successfully applied for TOMS data [Eck et al., 1995; Herman et al., 1996; Mayer et al., 1998a; Herman et al., 1999; Li et al., 2000], Global Ozone Monitoring Experiment (GOME) data [Peeters et al., 1998], and demonstrated for SBUV data [Frederick and Lubin, 1988; Soulen and Frederick, 1999]. Frederick and Lubin [1988] suggested the use of reflectivity from the solar backscattered ultraviolet (SBUV) instrument to derive average transmittance through clouds (SBUV FOV ~ 170 km by 170 km). Eck et al. [1995] used the higher spatial resolution TOMS data and obtained good comparisons with ground-based UV observations for snow-free conditions using a simple cloud correction method based on TOMS-derived reflectivity at 380 nm. It was also shown that TOMS reflectivity can provide estimates of monthly mean photosynthetically active (400–700 nm) radiation (PAR) [Eck and Dye, 1991] which compares with ground-based data as well or better than more customary techniques based on ISCCP cloud data [Dye and Shibasaki, 1995].

This paper describes the theoretical basis of the cloud correction method based on satellite UV reflectance data. It shows that the simple reflectivity technique [Eck et al., 1995] is a good approximation of the cloud transmittance in the UV

spectral region and how it can be improved to account for the wavelength-dependent attenuation due to clouds, effects of viewing geometry, and the presence of snow/ice. Section 2 presents a theoretical sensitivity study of the cloud transmittance and its relationship to the planetary albedo. Section 3 discusses two methods of estimating UV cloud transmittance from satellite UV reflectance measurements. Section 4 compares these satellite methods with cloud transmittance estimated from ground-based irradiance measurements for snow-free conditions. Snow effects are discussed in section 5. We also discuss briefly the effects of UV-absorbing aerosols embedded in clouds on estimating cloud transmittance (section 6). We restrict the current study to a homogeneous cloud model and Lambertian surface. In a subsequent paper we will estimate the errors in a homogeneous cloud model by applying a Monte Carlo analysis to estimate surface UV for various types of inhomogeneous cloud fields.

2. Relationship Between Cloud Albedo and Cloud Factor

The common approach for satellite estimations of surface irradiance involves calculation of a clear-sky surface irradiance, F_{clear} , multiplied by C_T (satellite-derived cloud and aerosol transmittance factor) to estimate the actual surface irradiance, F_{cloud} (see (1)):

$$F_{\text{cloud}} = F_{\text{clear}} C_T. \quad (1)$$

Calculation of F_{clear} from total ozone, extraterrestrial solar irradiance, and surface UV reflectivity was described in detail by Krotkov et al. [1998]. In this paper we assume that F_{clear} is known and focus on the theoretical estimation of C_T from satellite UV-reflectance measurements. We start this discussion with a simple theoretical model, which ignores the angular anisotropy of the radiation, molecular scattering, and ozone absorption. The atmospheric effects are considered later in section 2.2. Table 1 explains the main quantities used in this discussion.

2.1. Cloud Without Atmosphere

The key features for estimating C_T from satellite reflectance measurements can be understood while neglecting atmospheric effects and angular anisotropy of the radiation. Considering a simple model of a homogeneous cloud layer above a Lambertian reflecting surface, C_T can be formally expressed as a solution of the Stoke's problem [Chandrasekhar, 1960]:

$$C_T = C_{T0} = \frac{1 - R_C}{1 - R_S R_C^{\text{Diffuse}}}, \quad (2)$$

where R_S is the surface reflectivity (albedo), R_C and R_C^{Diffuse} are hemispherical albedos of the cloud layer illuminated by direct and diffuse source for zero surface reflectivity ($R_S = 0$) (see also Table 1). For a homogeneous cloud layer, R_C and R_C^{Diffuse} are unique solutions of the multiple-scattering radiative transfer problem for a given cloud optical thickness τ_C , single-scattering albedo ω_C , phase function γ_C , and solar zenith angle θ_0 . The solutions can be obtained either numerically or using analytical approximations (Figure 1), which allows calculation of C_{T0} for arbitrary R_S , θ_0 , and known cloud optical properties (τ_C , ω_C , γ_C) (Figure 2). Following this approach, one has to infer τ_C from satellite reflectance mea-

Table 1. Nomenclature

Symbol	Name	Definition	Comment
C_T	cloud transmission factor	equation (1)	different symbols in the literature: C_q [Chubarova, 1998]; f_g [Frederick and Lubin, 1988]; T [Frederick and Erlick, 1997]
C_{T0}	C_T without atmosphere	equation (2)	
R_C	hemispherical albedo of the homogeneous cloud layer	Figure 1	illumination by direct beam
R_C^{Diffuse}	same	Figure 1	illumination by isotropic diffuse source
R_{System}	hemispherical albedo of the cloud-surface system	equation (3)	see Figure 2 and Plate 3
R_{380}	Lambert equivalent reflectivity (LER) at 380 nm	equation (6)	for Rayleigh atmosphere and Lambertian surface: $R_{380} = R_{\text{system}}$ for $R_S > 0$ and $R_{380} = R_C$ for $R_S = 0$
S_b	diffuse reflection of Rayleigh atmosphere	equation (6)	illumination by isotropic diffuse source; similar to R_C^{Diffuse} but is spectrally dependent
R_S	surface reflectivity		surface is assumed Lambertian

surements (assuming cloud composition, geometry, and microphysics) and then calculate C_T directly from (2) using the same cloud model and assumed surface reflectivity.

Alternatively, one can first estimate the hemispherical albedo of the surface-cloud system from the measured satellite reflectance using a specified angular model of the reflected radiation [Li *et al.*, 2000]. Assuming that cloud scattering is conservative, there are no other atmospheric absorbers, and the surface albedo is known, C_T can be derived directly from the energy balance without retrieving cloud optical thickness and microphysical properties. Following this approach and ignoring effects of the angular anisotropy, the satellite reflectance is proportional to the hemispherical (planetary) albedo of the cloud-surface system, R_{system} , which can be expressed as a solution of the Stoke's problem:

$$R_{\text{system}} = R_C + \frac{T_C R_S T_C^{\text{Diffuse}}}{1 - R_S R_C^{\text{Diffuse}}}, \quad (3)$$

where T_C and T_C^{Diffuse} are cloud transmittances for direct and diffuse radiation. Equations (2) and (3) present a formal relationship between C_{T0} and R_{system} for an arbitrary surface reflectivity, solar angle, and arbitrary cloud parameters. The relationship becomes especially simple for the case of conservative scattering (nonconservative scattering is discussed in section 6). Assuming $T_C = 1 - R_C$ and $T_C^{\text{Diffuse}} = 1 - R_C^{\text{Diffuse}}$ in (2) and (3):

$$C_{T0} = \frac{1 - R_{\text{system}}}{1 - R_S} = 1 - \frac{R_{\text{system}} - R_S}{1 - R_S}. \quad (4)$$

Equation (4) is a consequence of the energy conservation for conservative cloud scattering. It shows that C_{T0} is proportional to $(1 - R_{\text{system}})$ with the slope inversely proportional to the

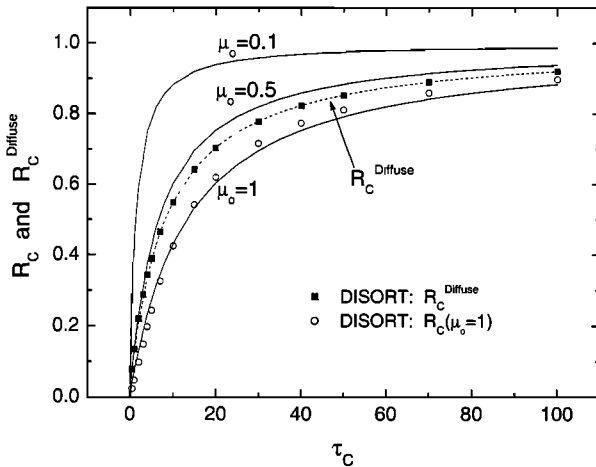


Figure 1. Cloud albedo R_C (solid lines) and R_C^{Diffuse} (dotted line) as a function of τ_C and $\mu_0 = \cos(\theta_0)$. The discrete points are from exact radiative transfer calculations (DISORT code [Stamnes *et al.*, 1988]), and the lines represent the two stream approximation [Coakley and Chylek, 1975]: $R_C = \tau_C^* / (\tau_C^* + 2\mu_0)$, $\tau_C^* = (1 - g)\tau_C$, $\mu_0 = \cos(\theta_0)$ and $R_C^{\text{Diffuse}} = 2 \int R_C(\mu_0) \mu_0 d\mu_0 = \tau_C^* [1 - 1/2 \tau_C^* \ln(1 + 2/\tau_C^*)]$, where $\tau_C^* = (1 - g)\tau_C$ is the cloud effective optical thickness, g is the asymmetry factor of the cloud phase function (for C1 model of the cloud droplet size distribution $g = 0.848$ [Deirmendjian, 1969]).

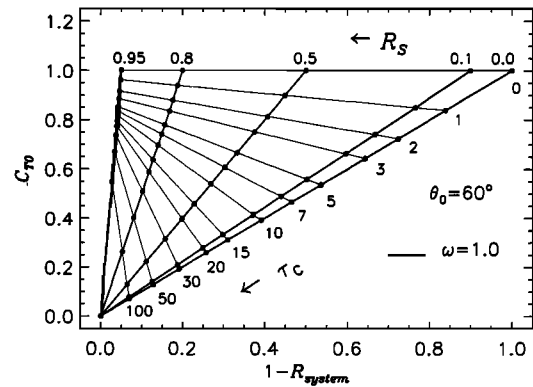


Figure 2. Relationship between C_{T0} and R_{system} for conservative scattering ($\omega_c = 1$) and different combinations of R_S , τ_C , and $\theta_0 = 60^\circ$. Here the abscissa shows the $1 - R_{\text{system}}$ value, and the C_{T0} is plotted on the ordinate. Thick solid lines represent the dependence of C_{T0} and R_{system} values on τ_C ($R_S = \text{const}$), and thin solid lines represent the dependence on R_S ($\tau_C = \text{const}$). The solar zenith angle is 60° , which is a typical value for winter months, when surface albedo substantially increases due to snow. C_T increases with increase in surface reflectivity but decreases with increase in cloud optical thickness (see Appendix A for discussion of enhanced cloud transmittance over snow).

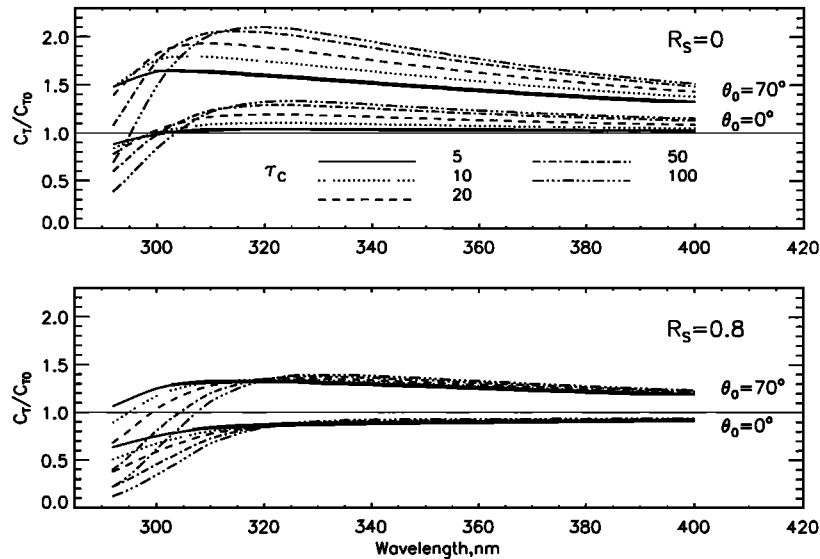


Figure 3. Spectral dependence of atmospheric effects on cloud transmittance, C_T/C_{T0} , for solar zenith angles 0° and 70° and different cloud optical depths. Zero surface albedo (top panel) and Lambertian surface with albedo 0.8 (bottom). The C1-cloud model embedded into molecular atmosphere (between 3 and 5.5 km) assuming 325 DU midlatitude ozone profile. The atmospheric scattering tends to increase C_T at UV-A wavelengths. At short UV-B wavelengths, absorption by tropospheric ozone has the opposite effect.

surface coalbedo. Calculations using DISORT results confirms this relationship, as shown in Figure 2, for different combinations of R_s and τ_c . Since in the near-UV spectral region R_s is uniformly low (1 to 8%) and spectrally flat for snow- and ice-free surfaces [Eck et al., 1987; McKenzie et al., 1996; Herman and Celarier, 1997], one can neglect surface reflection and determine C_T directly from cloud albedo:

$$\begin{aligned} C_{T0} &= 1 - R_{\text{System}} \\ R_{\text{System}} &= R_C. \end{aligned} \quad (5)$$

However, in the presence of snow ($R_s > 0.2$) the relationship between C_{T0} and R_{System} becomes more complex (Figure 2). Generally, increasing surface albedo causes C_{T0} and R_{System} to increase. On the other hand, increasing cloud optical thickness causes C_T to decrease, while R_{System} increases (except for enhanced cloud transmittance regime: $C_T > 1$ (see Appendix A)). Since the slope of C_T dependence on R_{System} increases with increasing surface albedo (see equation (4)) the C_T becomes increasingly sensitive to small errors in estimating R_{System} from satellite radiance measurements. Thus satellite C_T retrievals become increasingly noisy over bright surfaces (see examples in section 5).

2.2. Atmospheric Effects

The optical thickness of molecular atmosphere is larger in the UV spectral region than in the visible region ($\tau_R \sim 0.1$ at 500 nm and $\tau_R \sim 1$ at 300 nm), so the effects of molecular scattering cannot be neglected even for thick clouds. An additional complication arises from the strong spectral dependence of ozone absorption at short UV wavelengths ($\lambda < 320$ nm). To study the sensitivity of C_T to these atmospheric parameters, we consider a homogeneous water-cloud model embedded in a scattering molecular atmosphere with ozone absorption [Krotkov et al., 1997]. The optical thickness τ_c is assumed spectrally independent and that γ_c corresponds to the C1-cloud model

[Deirmendjian, 1969]. This cloud model is currently used in the TOMS operational UV algorithm [Herman et al., 1999].

To estimate the surface irradiance under an assumed cloud, we use both DISORT [Stamnes et al., 1988] (for large τ_c , where polarization can be neglected) and Gauss-Seidel code [Ahmad and Fraser, 1982] (for $\tau_c < 10$, where polarization can have an effect on backscattered radiances at the top of the atmosphere). C_T is then estimated from calculated surface irradiances according to (1) at a number of wavelengths in the UV spectral region (290–400 nm) for a wide range of cloud optical depths, surface albedo, and solar zenith angles.

Figure 3 shows the calculated spectral dependence of the ratio C_T/C_{T0} , where C_{T0} is the cloud transmittance without an atmosphere (discussed in section 2.1). Since our cloud model assumes spectrally independent cloud optical properties, C_{T0} does not depend on wavelength. However, the strong spectral dependence of Rayleigh scattering ($\sim \lambda^{-4}$) and ozone absorption in the UV-B spectral region (290–320 nm) causes C_T to be spectrally dependent [Nack and Green, 1974; Seckmeyer et al., 1996; Krotkov et al., 1997; Frederick and Erlick, 1997; Kylling et al., 1998]. The top panel in Figure 3 quantifies the effect for summer conditions, when surface reflection is small and can be neglected. In the UV-A spectral region (320–400 nm), where ozone absorption can be neglected, multiple reflections between the cloud layer and the Rayleigh atmosphere above and below the cloud make C_T larger than C_{T0} , similar to reflection from the ground (see equation (2)). Unlike the ground reflection, the fraction of reflected radiation backscattered to the cloud by the atmosphere increases at shorter UV-A wavelengths. The C_T enhancement is almost independent of the cloud altitude, but increases with solar zenith angle and cloud optical thickness, because of the increase in cloud albedo (Figure 1). At the shortest UV-B wavelengths ($\lambda < 300$ nm), tropospheric ozone absorption becomes so strong that it over-

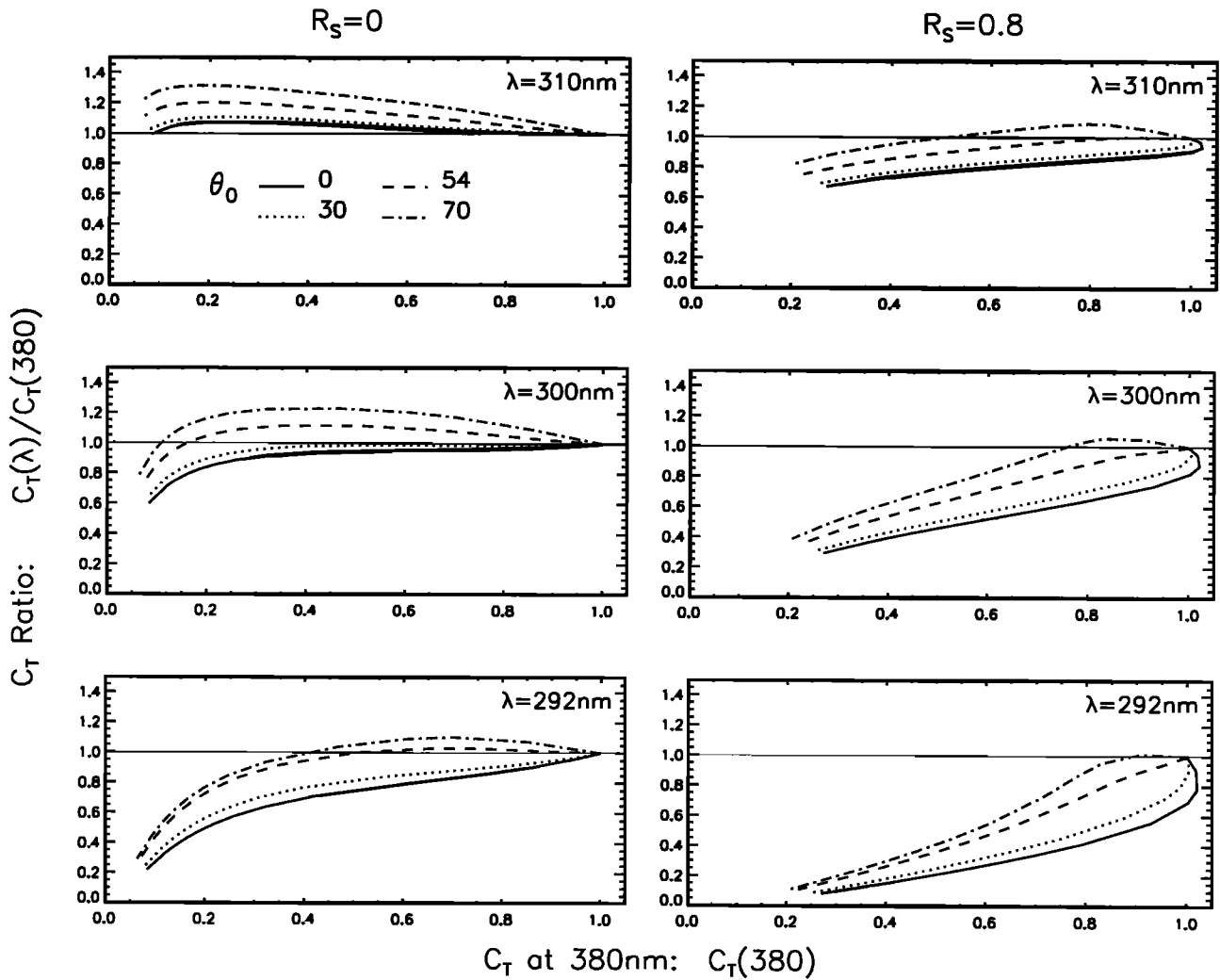


Figure 4. $C_T(\lambda)/C_T(380)$ ratio as a function of $C_T(380)$ at the wavelengths $\lambda = 310, 300$, and 292 nm. The same atmospheric and cloud models as in Figure 3.

comes the effect of Rayleigh scattering and reduces C_T compared to C_{T0} . Thus for a wide range of conditions, the spectral dependence of $C_T(\lambda)$ has a broad maximum around 310–325 nm.

In general, for a cloud over a dark surface, $C_T(\lambda)$ is a weak function of wavelength in the 300–400 nm spectral region. The spectral dependence of $C_T(\lambda)$ becomes even weaker over bright surfaces (Figure 3, bottom) because of the assumption of spectrally independent surface albedo. Because of this, $C_T(\lambda)$ can be estimated from a single spectral measurement (say C_T at 380 nm). From the practical point of view, C_T can be approximated directly from satellite estimates of R_{System} at one of TOMS reflectivity channels (360 or 380 nm) using (4) without inferring cloud optical thickness as an intermediate step. When the C_T is estimated at 380 nm (or 360 nm) it can be calculated at shorter UV-B wavelengths using a homogeneous cloud model and an average ozone profile (at least at wavelengths longer than ~ 310 nm, where tropospheric ozone absorption is weak (see Figure 4)). Therefore for satellite estimation of UV transmittance through homogeneous clouds, the problem of estimating C_T at all UV wavelengths is reduced to the estimation of cloud hemispherical albedo (R_{System}) at

one nonozone absorbing wavelength. We consider two practical solutions to this problem in section 3.

3. Satellite Estimation of C_T

In section 2.1 we have shown that at wavelengths, where we can neglect atmospheric effects, there is a linear relationship between the hemispherical albedo of the surface-cloud system and the cloud transmittance C_T , whose slope is determined by the surface reflectivity. In section 2.2 we showed that the atmospheric affects on C_T are relatively small even at UV wavelengths. Given the knowledge of C_T at one longer wavelength (say at 380 nm), one should be able to estimate C_T at shorter wavelengths (one known exception is thunderstorm clouds, where cloud geometrical thickness and tropospheric ozone inside the cloud becomes important [Mayer *et al.*, 1998b]). In this section we discuss two approaches for obtaining C_T , using satellite reflectance at a nonozone absorbing wavelength. We note that in the case of TOMS the reflectivity is determined from the radiance measurements at 380 nm for the Nimbus 7/TOMS (1978–1993) and at 360 nm in the case of Earth probe TOMS (1996 to present).

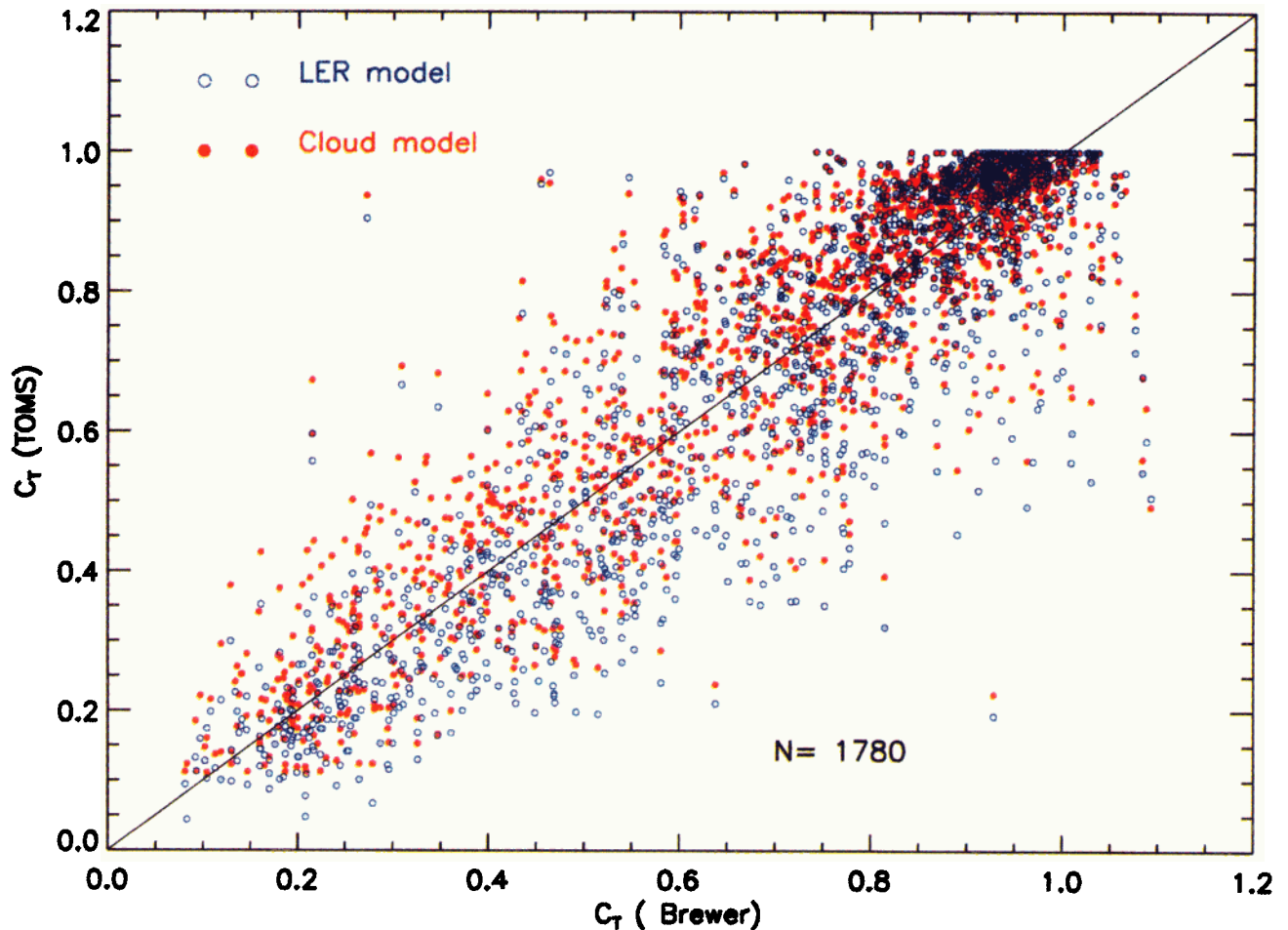


Plate 1. TOMS-derived C_T versus Brewer-measured C_T from daily measurements in Toronto, Edmonton, and Churchill during May to September 1989–1998. Correlation coefficient ~ 0.9 and standard deviation of the C_T difference about ~ 0.1 . TOMS estimates C_T by LER method (open blue circles) and cloud method (solid red circles). Brewer C_T measurements were averaged within ± 2 hours of the TOMS overpass time, while TOMS data represent instantaneous values for individual TOMS FOVs. The centers of all TOMS FOVs are within 35 km from the Brewer site.

3.1. LER Method

The first approach, proposed by *Eck et al.* [1995], is based on the Lambert equivalent reflectivity (LER), derived from the TOMS-measured radiance (I_{380}) near 380 nm. I_{380} can be expressed as a sum of the atmospheric backscatter above a specified Lambertian surface I_0 and the radiance reflected from this surface [*Chandrasekhar*, 1960; *Dave*, 1978; *Eck et al.*, 1987, 1995; *Herman et al.*, 1996]:

$$I_{380} = I_0(\theta, \theta_0, \varphi P_c) + \frac{R_{380} T_{380}(\theta, \theta_0, \varphi P_c)}{1 - R_{380} S_b(P_c)}, \quad (6)$$

where I_{380} and I_0 are the radiance to solar irradiance ratios, R_{380} is the Lambert equivalent reflectivity (LER) at 380 nm, S_b is the diffuse reflection of a Rayleigh atmosphere illuminated from below by an isotropic source, θ is the satellite zenith angle, θ_0 is solar angle, φ is azimuth angle, T_{380} is the total amount of direct plus diffuse radiation reaching the surface, multiplied by the atmospheric transmission of the diffuse reflected radiation in the direction of the satellite, and P_c is the surface pressure. For the wavelengths of interest, I_0 , S_b , and T_{380} are calculated assuming a pure Rayleigh atmosphere with

no gaseous absorption and no Mie scattering. A small correction is made for rotational-Raman scattering, using the procedure described by *Joiner et al.* [1995]. For the purpose of C_T estimation the surface pressure can be approximated by terrain pressure. This is a good approximation for broken cloud fields and thin semitransparent clouds. For thick clouds the I_{380} becomes insensitive to the cloud top pressure.

For partially cloudy fields of view the LER model (equation (6)) leads to a R_{380} dependence on wavelength *Hsu et al.*, 1997]. In the current TOMS (version 7) algorithm, two Lambertian reflecting surfaces are used, one for the ground (with an assumed reflectivity of 8%) and one for the cloud (with an assumed reflectivity of 80%). An effective cloud fraction is calculated from the measured 380 nm radiance. The effective R_{380} is then determined from the cloud fraction and assumed cloud and ground reflectivities [*McPeters et al.*, 1996]. The fractional R_{380} is close to but slightly less ($< 5\%$) than the standard R_{380} defined by (6). We will assume the standard definition of R_{380} (equation (6)) for the rest of the paper.

Eck et al. [1995] note that R_{380} thus obtained is approximately equal to the bidirectional reflectance of the clouds.

They are close because R_{380} is obtained by removing the atmospheric scattering component from the measured radiance using (6). However, the LER model imperfectly corrects for atmospheric scattering, and more importantly, the apparent cloud bidirectional reflectance is itself modified by atmospheric scattering. The cloud bidirectional reflectance can be expressed as a product of R_{System} and bidirectional anisotropic function, equal to unity for isotropic (Lambertian) reflection [Suttlles *et al.*, 1989]. At 380 nm the radiation reaching a cloud layer consists of both diffuse and direct components. The presence of the incident diffuse component effectively reduces the anisotropy of the scattered radiation, as the scattering of the outgoing radiation by the atmosphere. On the basis of these arguments one expects that R_{380} should be somewhat closer to the R_{System} (described in section 2.1) than the true cloud bidirectional reflectance is to R_{System} . Eck *et al.* [1995] also note that the TOMS instrument, in addition to its Sun-synchronous orbit near local noon, scans nearly perpendicularly to the principal plane of the Sun, which further reduces the effects of cloud anisotropy [Taylor and Stowe, 1984; Suttlles *et al.*, 1989]. Therefore if one makes a simplifying assumption that R_{380} is equal to R_{System} , one can use (4) to estimate C_T at 380 nm:

$$C_T(\text{LER}) = \frac{1 - R_{380}}{1 - R_S} = 1 - \frac{R_{380} - R_S}{1 - R_S}. \quad (7)$$

Equation (7) is a generalized form of Eck *et al.* [1995] model for an arbitrary surface reflectivity and can be applied to the clouds over snow if regional surface albedo (R_S) is independently known and $R_{380} > R_S$. Otherwise, if $R_{380} < R_S$, clear sky conditions are assumed and $C_T = 1$ (see section 5).

There are two sources of error in the LER method. One error comes from the difference between R_{380} and R_{System} and the other is due to the atmospheric effects on C_T , as described in section 2.2, which were not considered by Eck *et al.* [1995]. The last error would be reduced if R_{380} is actually less than R_{System} . In this case the $C_T(\text{LER})$ (estimated from (7)) becomes larger than C_{T0} (estimated from (4)), which effectively compensates for the real increase in C_T due to atmospheric scattering effects for $\lambda > 310$ nm (Figure 3). In Figure 5 we use our plane-parallel cloud model (described in section 2.2) to compare R_{380} with R_{System} for $R_S = 0$. The results show that for TOMS scanning geometry (in the plane perpendicular to the solar principal plane) the R_{380} is indeed less than R_{System} , which explains why the original LER technique works well for snow-free conditions.

3.2. Plane-Parallel Cloud Method

In Figure 6 we explicitly show the error in deriving C_T at 325 nm using the LER method (i.e., (7)) compared to the plane-parallel cloud method, which is currently used in the TOMS operational UV algorithm [Krotkov *et al.*, 1997; Herman *et al.*, 1999]. The cloud method uses the homogeneous cloud model (described in section 2.2) to calculate I_{380} for all satellite viewing conditions. The “effective” cloud optical thickness, τ_{eff} , is inferred by fitting the calculated and measured I_{380} . The τ_{eff} thus obtained would be equal to the real τ_C only in the idealized case of a plane-parallel homogeneous cloud layer. In the real case, τ_{eff} becomes a function of the assumed surface reflectivity, satellite observational geometry, cloud fraction and morphology, and solar zenith angle: $\tau_{\text{eff}}(\theta_0, I_{380}, R_S)$. As with the LER method, the value of R_S is taken from a climatological database of the minimal surface reflectivity that was de-

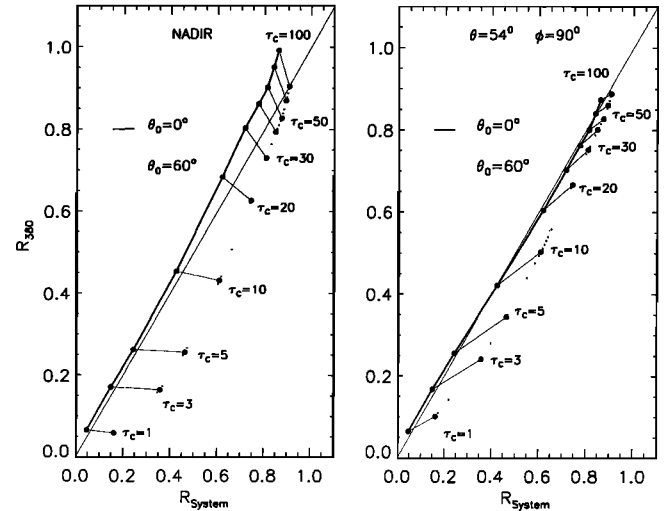


Figure 5. Relationship between TOMS reflectivity at 380 nm (R_{380}) and the hemispherical albedo of the cloud-surface system, R_{System} , for a C1 cloud embedded in a Rayleigh atmosphere for typical Nimbus-7/TOMS scanning geometry (left panel, nadir; right panel, edge of the swath 54° and azimuth angle 90°). For zero surface albedo, R_{System} is equal to the hemispherical cloud albedo R_C shown in Figure 1.

veloped using the 15 years of Nimbus-7/TOMS data [Herman and Celarier, 1997]. As a final step, the cloud model is used to calculate $C_T(\lambda, \tau_{\text{eff}}, R_S, \theta_0)$ at all UV wavelengths using a fixed climatological ozone profile and assuming that τ_{eff} is spectrally independent. Unlike the LER method, the cloud method explicitly accounts for the spectral dependence of C_T as well as cloud anisotropic reflectance.

As can be seen from Figure 6, the LER method tends to produce lower C_T values, except for large solar zenith angles and near-nadir observational directions. However, it should be noted that the plane-parallel cloud model itself is not neces-

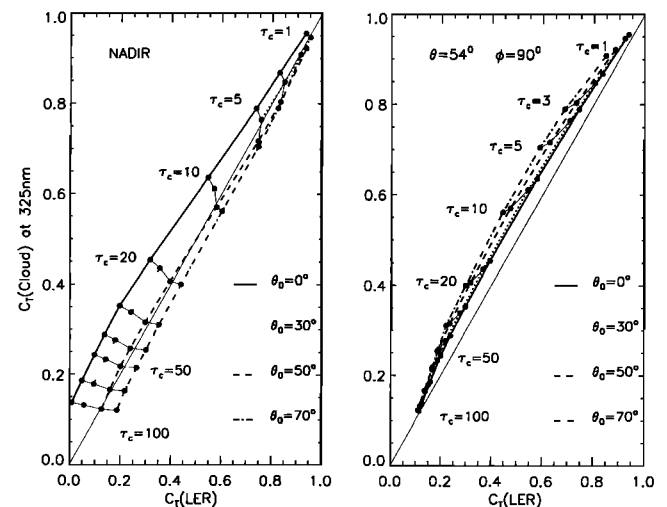


Figure 6. Comparison between two different methods of satellite C_T estimation: $C_T(\text{cloud})$ —plane-parallel cloud method and $C_T(\text{LER})$: Lambert effective reflectivity method. Wavelength 325 nm, solar zenith angles between 0° and 70° . Typical Nimbus-7/TOMS scanning geometry: left panel, nadir; right panel, edge of the swath and azimuth angle 90° .

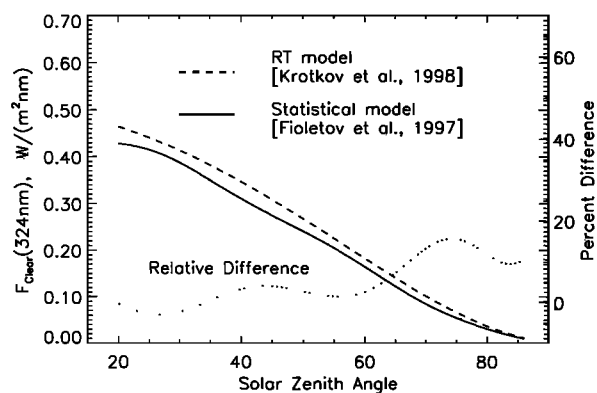


Figure 7. Clear-sky irradiance parameterizations, F_{clear} , at 324 nm for snow-free conditions: (a) statistical parameterization derived from all Brewer measurements based on 95% percentile method [Fioletov et al., 1997] (solid line) and (b) radiative transfer model for pure Rayleigh atmosphere (dashed line).

sarily an accurate representation of the true scattering from clouds. If real clouds are less anisotropic than predicted by the plane-parallel model, one would exaggerate the errors in the LER model. In section 4 we compare both methods with ground-based measurements of C_T .

4. Comparisons With Ground-Based Data

To compare satellite-derived C_T with ground-based observations, we first need a method of computing C_T from ground-based data. Brewer spectral UV measurements at three Canadian sites, Toronto, Edmonton, and Churchill, taken between 1989 and 1998, were used for comparisons. The Brewer instrument measures horizontal, spectral UV irradiance with a spectral resolution of ~ 0.55 nm, full width at half maximum (FWHM). In its normal UV routine, the Brewer scans from 290 to 325 nm with ~ 0.5 nm steps. There are normally from one to four such measurements performed every hour throughout the day from sunrise to sunset. The 324 nm wavelength was used for the cloud transmission comparison. The ozone absorption is the smallest at that wavelength in the Brewer spectral range.

4.1. Clear-Sky Irradiance Parameterization

The Brewer cloud factor is a ratio between the measured UV irradiance at 324 nm and the “clear-sky” parameterization. The statistical “clear sky” irradiance (F_{clear}) was parameterized on the basis of a 95 percentile method: when the measured irradiance data (after the Earth-Sun distance adjustment and for no-snow conditions) are compared to F_{clear} for each solar zenith angle, $\sim 95\%$ of all data are less than F_{clear} and 5% are more than F_{clear} [Fioletov et al., 1997]. A statistical approach based on a 95 percentile gives results that are reasonably close to the model calculations for a pure Rayleigh atmosphere (Figure 7), although it may introduce some systematic bias in C_T comparisons.

Figure 7 shows that F_{clear} estimation from a radiative transfer (RT) model is ~ 10 – 15% higher than Brewer statistical F_{clear} estimation at solar zenith angles less than 65° . At least part of this bias is due to the cosine error, which reflects the fact that Brewer spectrometers are calibrated at normal incidence, and their responsivity decreases with increasing zenith

angle [e.g., Bais et al., 1998]. Therefore F_{clear} measured by Brewer is less than that falling on a horizontal surface, and positive correction is required. Estimates of the Brewer correction from Toronto and other Canadian stations are given as $+6\% \pm 2\%$ (bias ± 1 standard error) and $+6\% \pm 3\%$, respectively. After the cosine correction an average systematic difference between the Brewer statistical model and the RT model becomes less than 8% for solar zenith angles less than 65° . This error is larger than Brewer-model differences for completely cloud-free days (the RT model is ~ 2 – 4% higher after aerosol and cosine corrections [Krotkov et al., 1998]) and is comparable to the differences between the 95 and the 99 percentile methods (the 99 percentile gives about 8% higher values for Brewer F_{clear}). In this paper we focus on the comparisons of cloud transmittance. Comparing C_T values (see (1)) reduces the instrument-calibration bias, to an extent that it is the same for clear and cloudy conditions.

4.2. Random Differences

Daily TOMS estimates of C_T (section 3) were compared with ground-based Brewer spectrometer measurements of the same quantity (Plate 1). The comparisons were done under conditions without snow or ice (snow effects are discussed in section 5). Direct comparison of C_T estimated from a low-resolution satellite instrument, such as TOMS, and ground data is difficult because TOMS has roughly a diamond-shape ground field of view (FOV) with sides that vary from about 50 km \times 50 km at nadir to 100 km \times 250 km in the extreme off-nadir direction. By contrast, ground-based UV-B observations are primarily influenced by clouds within a circle of few kilometers radius. There is always some random error in Brewer estimates of C_T (e.g., short-term variations in cloud conditions). To reduce the standard deviation of C_T , several Brewer measurements close to TOMS overpass time were averaged together. We found for the Toronto location that standard deviations are 37, 26, and 21% for 1 hour, 2 hour, and 4 hour averaging, respectively. The corresponding correlation coefficients are 0.8, 0.87, and 0.9, respectively. The time averaging has little effect on the slope of the regression line: $C_T(\text{TOMS}) = AC_T(\text{Brewer})$. Six hour averages had larger standard deviations than 4 hour averages because differences in local time and solar zenith angle between the Brewer and the TOMS measurements were too large. Therefore the Brewer data in Plate 1 represent the 4 hour averages. The TOMS data represent individual FOVs (with centers less than 35 km from Brewer station) for the period 1989 to June 1998 and are from both Nimbus 7/TOMS (1979 to May 1993) and Earth probe/TOMS (August 1996 to December 1998).

The correlation between TOMS and Brewer C_T values improves with decreasing distance between the center of the TOMS FOV and Brewer location and the size of the TOMS FOV. In 1996–1997 the Earth probe TOMS was placed in a low orbit, which resulted in smaller FOV (~ 26 km in nadir). Selecting this subset of the TOMS data resulted in an increased correlation with Brewer measurements at Toronto (correlation coefficient ~ 0.95 for 82 points) compared with the Nimbus-7 TOMS data (~ 50 km in nadir) for the same location (correlation coefficient ~ 0.91 for 215 points). However, restricting the distance and size of the satellite FOVs results in considerable reduction in data pairs available for comparisons, which undermines statistical confidence of the results. Therefore the restrictions on the TOMS data (Plate 1) were relaxed to allow all sizes of TOMS pixels if the distance between the

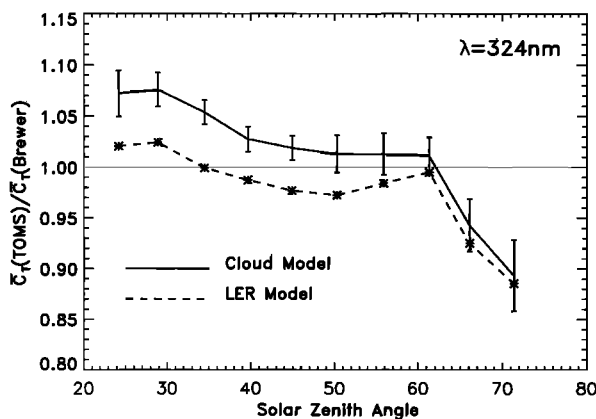


Figure 8. Ratio of the mean TOMS and Brewer C_T values binned by solar zenith angle (5° bins). The solid line represents operational TOMS C_T estimate based on a plane-parallel cloud model. The dashed line represents the old TOMS C_T estimate based on the LER model [Eck et al., 1995]. The error bars are 2 times the standard error of the mean C_T ratio in a given bin.

center of TOMS and the Brewer FOVs is less than 35 km. The additional restrictions are solar zenith angle less than 75° as well as absence of snow (according to both TOMS and ground data) and absorbing aerosols (TOMS aerosol index less than 0.5). Since we found no significant differences between Brewer locations, all stations were analyzed together. The combined data set of Brewer-TOMS C_T pairs includes 1780 points with the C_T correlation coefficient ~ 0.9 (Plate 1).

4.3. Systematic Shifts

The variance in the C_T daily comparisons is large (the standard deviation of the absolute C_T difference is about 0.1) mostly because of the different scales of the ground and satellite FOVs. Therefore to obtain meaningful comparisons, one must average the data. One way to do so is to bin both data sets by solar zenith angle (SZA). From (1), since F_{clear} is relatively constant within a narrow solar zenith angle bin, the average irradiance at the ground is determined essentially by the average value of C_T . Figure 8 shows the comparison of average values of C_T derived from ground-based observations with the two satellite methods described earlier. The plane-parallel cloud model tends to overestimate C_T by about 7% at small SZA but underestimates it by up to 15% at large SZA. If this result is added to the 10% bias between satellite and uncorrected Brewer data for clear-sky conditions (Figure 7), one gets an SZA-dependent total bias that changes from +20% at low SZA to nearly zero at high, consistent with the pattern noticed by Herman et al. [1999]. Surprisingly, the simpler LER method agrees a bit better with ground data at low solar zenith angles than the more sophisticated plane-parallel cloud method. One possible explanation for this result is that at low solar zenith angles real clouds, on aggregate, behave more like a Lambertian reflector in a TOMS FOV than a plane-parallel cloud. The discrepancy at large solar zenith angles is currently not understood. We plan to conduct Monte Carlo studies to see if broken cloud models can resolve this discrepancy.

Another way to compare satellite and ground-based C_T is to group the data into narrow C_T bins. Figure 9 shows such a comparison. Note that the largest value of C_T observed from Brewer exceeds 1. This is a well-known feature in ground

observations, caused by reflection of direct solar radiation from the sides of clouds providing a larger ground irradiance than would be obtained if the clouds were not there [Nack and Green, 1974; McCormick and Suehrcke, 1990; Mims and Fredrick, 1994; Chubarova, 1998]. Since there is no way to estimate this effect from satellite observations using homogeneous cloud models, satellites would always tend to underestimate C_T when the sky consists of small amounts of broken clouds. Figure 9 also shows that the plane-parallel cloud model tends to overestimate C_T at smaller C_T , i.e., in the presence of thick clouds. Again, surprisingly, the LER model does a bit better.

One problem in these comparisons is that there is an inherent statistical bias that occurs even if both data sets were to be perfect in their own viewing domains. For example, when Brewer sees 5% cloud cover, the minimum TOMS can see is 0%, but maximum can be close to 100%. This creates a highly asymmetric long-tailed probability distribution function (caused by imperfect spatial and temporal coincidence between satellite and ground instruments), which will tend to bias the average cloud cover seen by TOMS too high relative to Brewer, even if both Brewer and TOMS are reporting the correct amounts in their FOVs. An opposite problem occurs when the cloud amounts are close to 100%. TOMS would tend to report less than 100% cloudiness when Brewer sees 100% cloud cover. Note that the problem reverses if one bins the C_T data with TOMS-observed cloud amounts and finds the mean Brewer C_T in each bin. Now the Brewer would see too much cloud in the low-cloud TOMS bins, and vice versa. It is likely that some of the difference between TOMS and Brewer C_T in Figure 9 is caused by this effect.

A practical solution to the problem of large daily scatter between satellite and ground C_T estimates (when the satellite FOV cannot be reduced) is to consider weekly and monthly C_T averages (this is similar to using 7 day running averaging by Herman et al. [1999]). As expected, the scattering of monthly and daily averages is substantially smaller than for daily values. The standard deviation of the difference between TOMS and Brewer C_T values is about 0.06 for weekly means and 0.04 for monthly means. For most months the agreement is sufficiently close to be useful for validation of the ground-based Brewer measurements. Using running averages of the monthly means

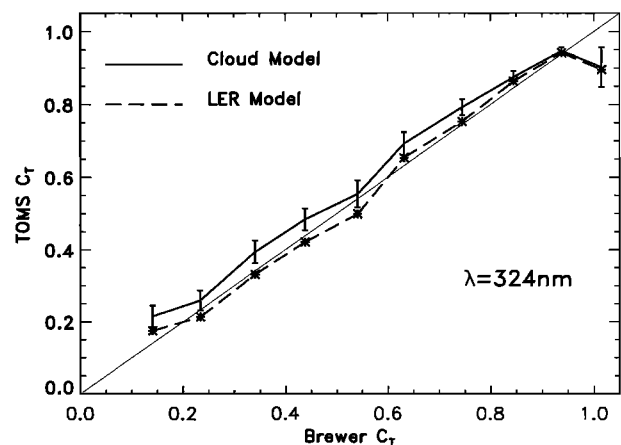


Figure 9. TOMS and Brewer C_T binned by Brewer C_T values (0.1 bins). The solid line represents current TOMS C_T estimate based on a plane-parallel cloud layer. The dashed line represents the old TOMS C_T estimate based on the LER model [Eck et al., 1995].

brings the agreement within a few percent that is reasonably close to the instrument calibration uncertainty and well below large instrument absolute calibration drifts occasionally seen in the ground-based network.

5. Clouds Over Snow

While the largest doses of UV irradiance usually occur during the summer months, the sensitivity of biological systems to UV dosage also varies with season. For some organisms the maximum sensitivity occurs near the end of winter and during the spring months, while the organisms are immature and in their maximum growth phases. In many regions, this requires consideration of the effects of snow and ice combined with clouds to estimate the UV dosage and long-term changes from historical values. These effects are especially important over the large landmass at higher latitudes in the Northern Hemisphere (northern Europe and Canada), mountain regions everywhere, in southern Chile and Argentina, and near the Arctic and Antarctic ice shelf (for marine life). The presence of clouds and snow causes the most difficult conditions for the accurate estimation of UV irradiance.

The presence of snow causes increases in surface irradiance under clear sky and even more under cloudy conditions [Lubin *et al.*, 1994; Lenoble, 1998; Herman *et al.*, 1999; WMO, 1999; Kylling *et al.*, 2000]. Assuming Lambertian reflectance, the TOMS algorithm can properly account for conservatively scattering clouds over snow/ice if the snow albedo is known from outside data (see (1) and (7)):

$$F(\text{snow}) = \left[\frac{F_{\text{Clear}}(R_s = 0)}{1 - R_s S_b} \right] \left[\frac{1 - R_{380}}{1 - R_s} \right], \quad (8)$$

where R_s is the FOV average (regional) snow albedo, $S_b(\lambda)$ is the wavelength-dependent fraction of radiation backscattered from the Rayleigh atmosphere back to the surface, R_{380} is the TOMS-measured LER at 380 nm (equation (6) and Table 1), and $F_{\text{Clear}}(R_s = 0)$ represents clear-sky irradiance for zero surface albedo. The current TOMS algorithm uses a climatological snow/ice flag (probability of the presence of snow on a given day at a given location) and an assumption about constant surface reflectivity in the presence of snow/ice ($R_s = 0.4$ for all locations). Any additionally measured scene reflectivity is assigned to a cloud. The value $R_s = 0.4$ was selected as appropriate for snow-covered urban/suburban-populated areas containing at least moderate densities of roads, houses, and trees (e.g., Toronto). The value is known to be wrong for freshly fallen snow, remote mostly flat areas [Grenfell *et al.*, 1996], and areas where the snow cover is almost total over extended periods (e.g., Edmonton, Churchill). Underestimation of the snow albedo at high latitudes results in an underestimation of C_T and UV irradiance [Kalliskota *et al.*, 2000] (see Plate 2, top panel).

The first-order correction to the TOMS UV algorithm is to use regional snow albedo values, which are different for different locations. It is now possible to derive the regional snow albedo climatology from ground-based measurements combined with satellite data. For example, the UV regional snow albedo can be inferred from TOMS reflectivity measurements on cloud-free days with snow ($R_s = R_{380}$). Plate 2 shows frequency distributions (histograms) of TOMS reflectivity measurements for all-sky and separately for clear-sky days for three selected Brewer sites: Toronto (43.78°N), Edmonton

(53.55°N), and Churchill (58.75°N). The days with snow were selected using actual snow-depth measurements available from each site. The cloud screening was performed using Brewer UV measurements for each site using the following algorithm. First, all Brewer observations taken under clear-sky conditions have been divided into two groups: with and without snow cover. Comparing Brewer observations with and without snow, it was previously shown that on average, snow enhances clear-sky flux at 324 nm by $\eta \sim 1.39$ at Churchill, $\eta \sim 1.21$ at Edmonton, and $\eta \sim 1.12$ at Toronto [Fioletov and Evans, 1997]. To estimate C_T in the presence of snow, measured UV irradiance at 324 nm, $F_{324}(\text{snow})$ was divided by “statistical clear-sky” Brewer irradiance parameterization ($F_{\text{Clear}}(\text{no snow})$, Figure 7) multiplied by the mentioned above amplitudes of snow enhancement, η :

$$C_T(\text{Brewer}) = \frac{F_{324}(\text{snow})}{F_{\text{clear}}(\text{snow})} = \frac{F_{324}(\text{snow})}{\eta F_{\text{clear}}(\text{no snow})}. \quad (9)$$

Finally, the clear days were identified using (9) and the condition $C_T(\text{Brewer}) > 0.9$. On cloud-free days the TOMS-measured reflectivity is representative of the regional snow reflectivity: $R_s = R_{380}$. The histograms of R_{380} for each site are shown in the bottom part of Plate 2. The larger histograms include both clear and cloudy days, and the smaller ones include only clear days according to the Brewer cloud-screening technique described above (i.e., $C_T(\text{Brewer}) > 0.9$). We see that the mean R_s value increases, and the R_s variability decreases when one compares locations from Toronto to Churchill. The mean $\langle R_s \rangle$ values are also shown in the lower panels of Plate 2 as vertical blue bars ($\langle R_s \rangle = 0.53$ for Toronto, $\langle R_s \rangle = 0.58$ for Edmonton, and $\langle R_s \rangle = 0.78$ for Churchill stations). One can use these calculated values as a new estimate of R_s when estimating UV irradiance from the TOMS reflectivity data using (8).

The results of C_T comparisons are summarized in the top part of Plate 2 using both the current TOMS method ($R_s(\text{curr}) = 0.4$) and the new values, $R_s(\text{new})$, which are different for each site. Although all stations show approximately the same high correlation between TOMS and Brewer C_T for no-snow conditions ($r \sim 0.9$), the correlation becomes progressively worse with increasing average regional snow albedo ($r = 0.68$ for Toronto, $r = 0.44$ for Edmonton, and $r = 0.12$ for Churchill). Changing R_s value does not improve the correlation between TOMS and Brewer C_T . However, it affects strongly the bias between TOMS and Brewer C_T estimates.

In terms of bias the current TOMS R_s value ($R_s = 0.4$) actually works better than the new value ($\langle R_s \rangle = 0.53$) for the Toronto location. Using the current value for R_s , TOMS only slightly overestimates C_T for thick clouds (small $C_T(\text{Brewer})$) and underestimates C_T for thin and broken cloud conditions. Overall, the $R_s = 0.4$ value seems to be a reasonable compromise if one chooses to use a single value during the entire snow season for Toronto. The new $R_s = 0.53$ value systematically overestimates C_T for all-sky conditions, except for almost clear-sky conditions ($C_T(\text{Brewer}) > 0.95$). This is probably an indicator of measurable differences in snow regime between the Brewer location and the larger surrounding area (the average TOMS FOV ~ 100 km). If the goal is to get the best comparison between satellite and Brewer UV flux, it is better to use the current TOMS R_s value for Toronto. The close value of $R_s(\text{Brewer}) \sim 0.35$ can be also estimated from (8) using $\eta = 1.12$ [Fioletov and Evans, 1997] and is close to the TOMS estimate $R_s(\text{Brewer}) \sim R_s(\text{TOMS}) = 0.4$.

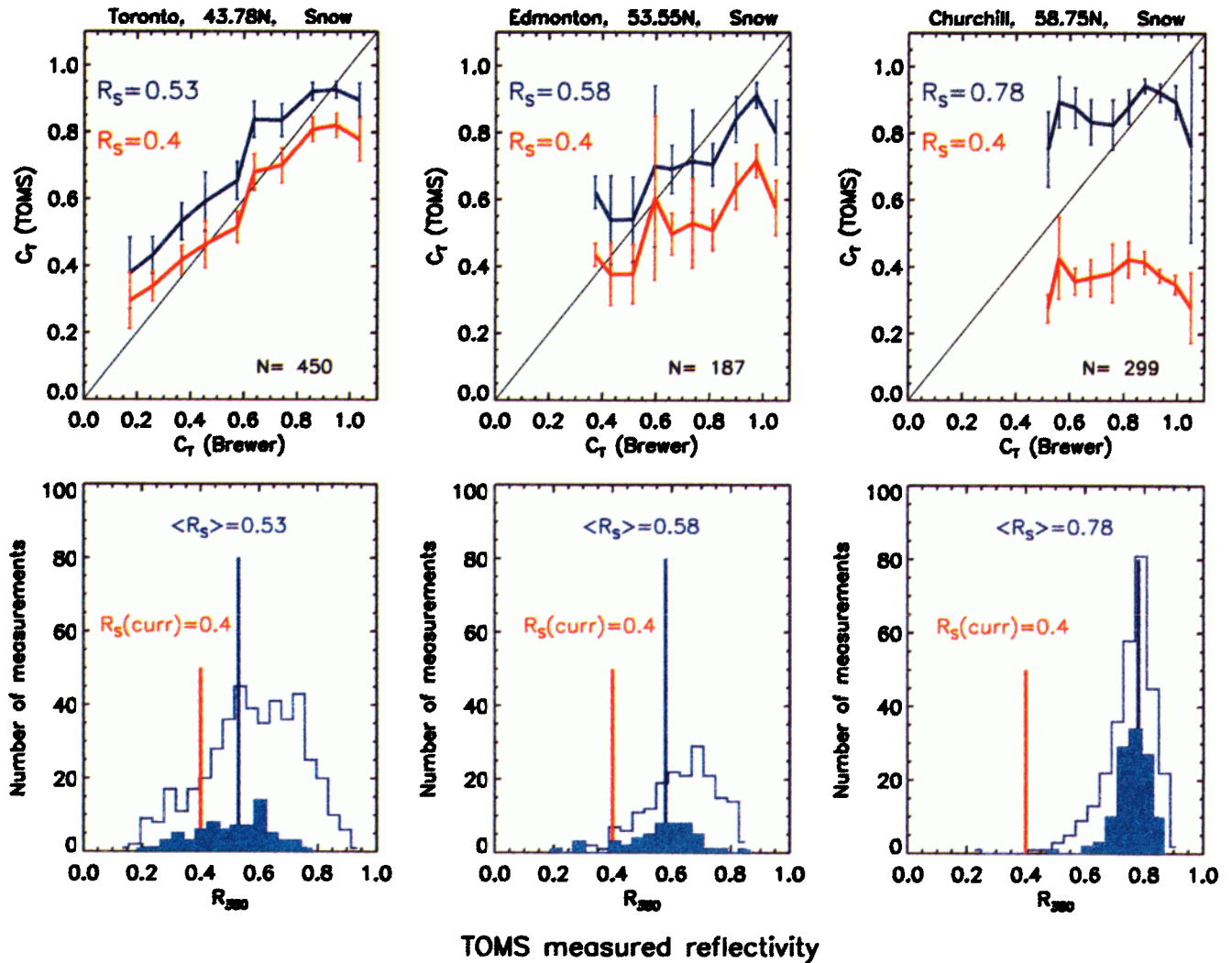


Plate 2. (top) TOMS versus Brewer C_T binned by Brewer C_T values (same as Figure 9 but for snow conditions and separately for Toronto, Edmonton, and Churchill locations). The red line represents current TOMS C_T estimate assuming constant snow albedo $R_S = 0.4$ for all locations, and the blue line represents TOMS C_T assuming the true average regional snow albedo, which is different for each location ($\langle R_S \rangle$; see bottom panel). The error bars are 2 times the standard error of the mean TOMS C_T in a given bin. (bottom) histograms of the TOMS reflectivity measurements, R_{380} , for snow days for each site. The larger histograms represent all-sky conditions (clouds over snow) and smaller filled histograms represent clear-sky conditions with snow, when R_{380} is representative of the regional snow albedo in the TOMS FOV. The vertical blue bars represent seasonally average snow albedo for each site, $\langle R_S \rangle$. The current TOMS snow albedo ($R_S(\text{curr}) = 0.4$ for all sites) is shown as a red vertical bar.

The situation is quite different for high-latitude locations (Edmonton and Churchill), where $R_S(\text{curr})$ causes systematic C_T underestimation for all conditions. For these sites using new regional snow albedo values allows to reduce the average bias between $C_T(\text{TOMS})$ and $C_T(\text{Brewer})$ (see Plate 2). However, using a single value for R_S for all conditions does not improve the correlation between $C_T(\text{TOMS})$ and $C_T(\text{Brewer})$ on a daily basis.

The main source of discrepancies between TOMS and Brewer C_T estimates is the daily variability of the regional snow albedo. Suppose on one day the $R_S(\text{TOMS}) \sim R_S(\text{Brewer}) \sim R_S(\text{true})$, and both TOMS and Brewer give close estimates of C_T . Suppose there is a fresh snowfall on the next day, but cloud conditions stay the same. Since fresh snow increases both surface irradiance and backscattered radiance, TOMS would

assume thicker cloud on that day and reduce $C_T(\text{TOMS})$, while Brewer would assume thinner cloud and increase the $C_T(\text{Brewer})$. We can estimate the error in the TOMS flux due to error in R_S by taking the derivative of (8):

$$\frac{\Delta F}{F} = \left(\frac{S_b}{1 - R_S S_b} + \frac{1}{1 - R_S} \right) \Delta R_S, \quad (10)$$

where $\Delta R_S = R_S(\text{assumed}) - R_S(\text{true})$ is the error in satellite estimated R_S . The first term accounts for error in F_{Clear} , and the second one accounts for error in C_T . Figure 10 shows both the total error and, separately, the errors in F_{Clear} and C_T as a function of R_S . We note that the total error is dominated by the C_T error, which increases by an order of magnitude with R_S increase from zero to >0.9 . We also note that errors in C_T and R_S are of the same sign: underestimation of R_S (fresh

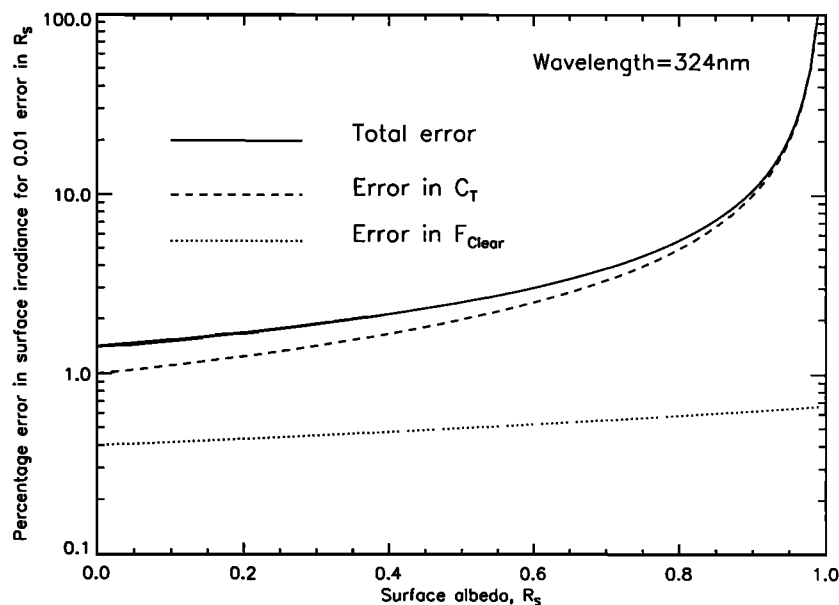


Figure 10. Percentage error in surface irradiance at 324 nm for 0.01 error in surface albedo R_s as a function of R_s . The error is a sum of the F_{Clear} error (dotted line) and C_T error (dashed line). We assume Lambertian reflection, so the error is not a function of solar angle. The error in surface irradiance is dominated by C_T error for all but snow-free conditions.

snowfall) causes underestimation of C_T (TOMS) and vice versa. This explains progressively worse results of comparisons from Toronto to Churchill when using the fixed value of $R_s = 0.4$.

In addition to the site-to-site variability, the albedo at individual sites can vary depending on the age and depth of snow as well as surface temperature [Schwander *et al.*, 1999]. One can see that the variability in R_s (width of the clear sky R_{380} histograms in Plate 2) decreases from Toronto to Churchill (with Edmonton showing intermediate albedo and variability). Both Edmonton and Churchill instruments are located at rural sites, so the difference is not due to urban influences and is probably due to differences in terrain (flatness, trees). Currently, for sites with high surface albedo during winter months, TOMS can only estimate the average monthly flux with almost no correlation on the daily basis. This would be improved by developing regional snow albedo climatology, which should also be time dependent. For estimation of UV irradiance, averaging the transmittance over at least a week should minimize errors caused by fresh-snow conditions compared to the true weekly dosage. Accurate daily TOMS estimation of UV irradiance would require a priori knowledge of the surface reflectance for all conditions.

6. Nonconservative Cloud Scattering

For satellite estimation of cloud transmittance in the visible and near-UV spectral regions, a conservative-scattering regime is usually assumed (cloud single-scattering albedo, $\omega = 1$). Calculations [Twomey, 1972; Twomey and Bohren, 1980; Twohy *et al.*, 1989; Chylek *et al.*, 1996] and direct measurements [King *et al.*, 1990] of the cloud single-scattering albedo show that this is a reasonable assumption at least for clean marine clouds ($\omega > 0.9999$). Yet other measurements suggest that some absorption is possible at visible and near-UV wavelengths for polluted clouds (e.g., a mixture of clean-water droplets with

absorbing aerosols possibly containing soot) [Melnikova *et al.*, 1994; Wendisch and Keil, 1999]. A thorough treatment of absorbing aerosols mixed with cloud droplets on UV cloud transmittance requires a rather complicated model, which combines detailed cloud and aerosol microphysics with an accurate radiative transfer scheme, and is a subject of ongoing research [Erlick *et al.*, 1998]. In this section we use a simplified model to examine qualitatively the effect of cloud pollution on satellite C_T estimation for a snow-free and snow conditions.

There are two additional sources of error in satellite C_T estimation for polluted clouds. First, polluted clouds transmit less radiation to the ground than conservative clouds for the same satellite reflectance [Wendisch and Keil, 1999]. Second, polluted clouds modify the spectral dependence of C_T [Erlick *et al.*, 1998]. To examine the first effect, let us neglect atmospheric scattering and assume that cloud single-scattering albedo ω_c is independent of cloud optical thickness (e.g., the cloud is homogeneous and cloud droplets and soot particles are internally mixed). Plate 3 shows the relationship between C_{T0} and R_{System} for both conservative ($\omega = 1$) and nonconservative ($\omega = 0.999$) cloud scattering. For polluted cloud and snow-free conditions, R_{System} increases with τ_c but never gets larger than $\sim 80\%$ even for very thick cloud ($\tau_c > 100$). On the other hand, for nonconservative clouds over fresh snow, the reflectivity of the scene (R_{System}) decreases with increases in cloud optical thickness because of multiple reflections from the surface and losses within the cloud. For the intermediate snow reflectivity ($R_s \sim 0.6$ – 0.8), R_{System} does not change with τ_c , while C_T changes from 1.1 to almost zero. This means that the satellite reflectance measurements are not useful for determining nonconservative C_T over bright snow surfaces ($R_s > 0.5$) even if R_s is known a priori. For snow-free conditions, satellite reflectance method overestimates C_{T0} by assuming a conservative cloud model. The error is small for

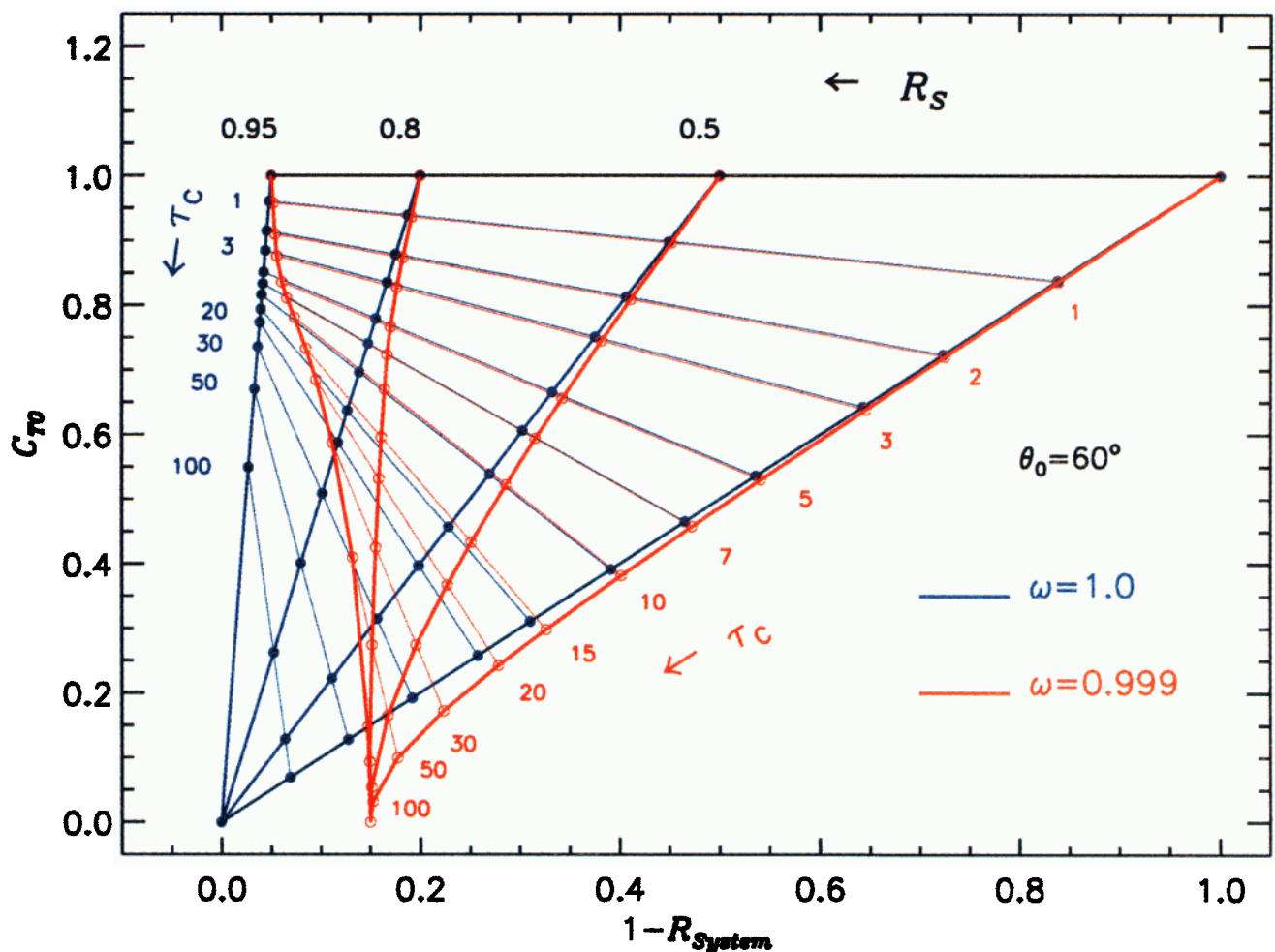


Plate 3. Relationship between C_{T_0} and coalbedo of the “cloud-surface” system, $1 - R_{\text{System}}$ using DISORT [Stamnes *et al.*, 1988] for a conservative C1-cloud layer (solid blue lines and circles) and nonconservative cloud ($\omega = 0.999$, red lines and open circles). Lambertian reflective surface with reflectivity R_s between 0 and 0.9, solar zenith angle 60° (same as Figure 2).

cloud optical thickness less than 10 but increases with cloud optical thickness.

The second source of error for polluted clouds is from the modification of the spectral dependence of C_T . To gain a qualitative understanding of this effect, we embedded a conservative cloud layer into an atmospheric model with a preexisting absorbing (dust) aerosol profile (Gaussian layer with peak height at 3 km and half width of 1 km). The cloud altitude was from 3 to 5.5 km. Therefore roughly half of the aerosol layer was mixed with cloud with no aerosol above the cloud. We assume external mixture of water drops and dust particles and no physical interaction between dust particles and cloud droplets. The dust aerosol model is similar to the Dust 2 model described by Krotkov *et al.* [1998] with single-scattering albedo ~ 0.6 and unit optical thickness at 325 nm. Figure 11 shows the spectral dependence of C_T for a pure water cloud, for a dust aerosol layer, and their mixtures at UV-A wavelengths and solar zenith angle 50° . We see that the C_T spectral dependence for dust aerosol is opposite to that of a pure water cloud: C_T decreases at shorter UV-A wavelengths. This spectral behavior is similar to urban aerosols often found in industrial areas [Erlick and Frederick, 1998]. We see from Figure 11, that highly absorb-

ing and optically thick aerosol layer mixed with a thin cloud of approximately equal optical thickness can invert the spectral dependence of C_T of the mixture. Erlick *et al.* [1998] shows a similar effect for an optically thin stratus and an urban aerosol profile. For optically thick clouds mixed with absorbing aerosols, the shape of C_T spectral dependence tends to be flatter than for conservative clouds (Figure 11). Therefore the satellite method of estimating C_T using a plane-parallel conservative cloud model tends to overestimate C_T not only at the reflectivity wavelength (380 nm) but also at the shorter UV wavelengths. However, it still needs to be shown that polluted clouds do occur systematically for any region and that aerosol (soot) concentration is high enough to produce substantial deviation in the cloud single-scattering albedo (0.999 or less) for optically thick clouds. Better understanding of the C_T spectral dependence at UV-A wavelengths is required for understanding limitations of the satellite UV measurements. Ground-based instruments simultaneously measuring global irradiance at least at two different wavelengths in the UV-A region can help achieve this.

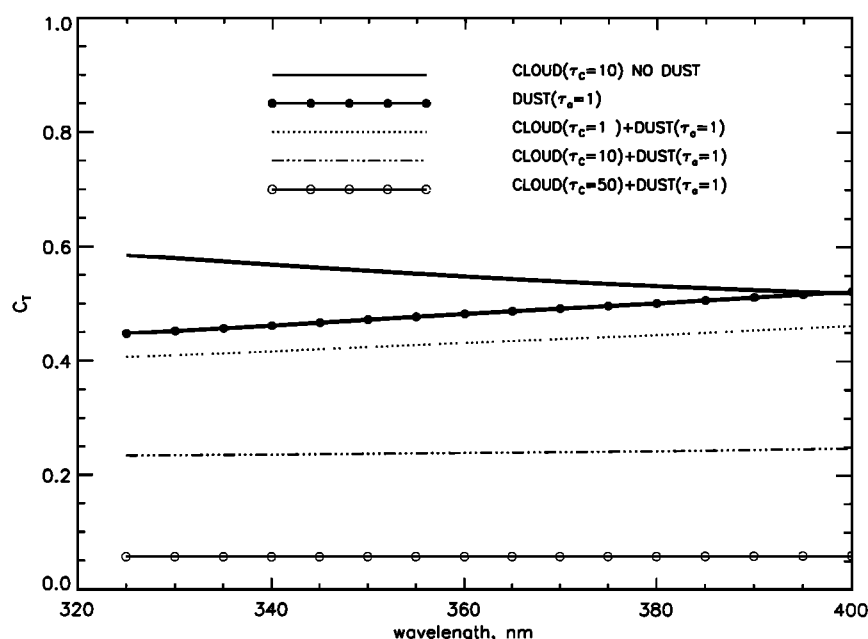


Figure 11. Spectral dependence of C_T for external mixture of cloud drops and absorbing (dust) aerosol particles. The dust aerosol model is similar to the Dust 2 model described by Krotkov *et al.* [1998] with unit optical thickness at 325 nm. The C_T spectral dependence for dust is opposite to that of the pure water cloud. Cloud drops dominate the shape of the spectral dependence of the mixture, unless the cloud optical thickness is close to aerosol optical thickness. Solar zenith angle is 50° .

7. Summary

Radiative transfer calculations and simplified analytical expressions have been presented for the convenient estimation of the transmission of ultraviolet radiation through plane-parallel clouds over a surface with arbitrary reflectivity R_s . The main results can be summarized as follows:

1. For conservative cloud scattering over snow-free surfaces, at wavelengths where one can neglect atmospheric scattering and absorption effects, it was demonstrated that there is a linear relationship between the hemispherical albedo of the surface-cloud system and the cloud transmittance C_T (the ratio of cloudy to clear-sky surface irradiance), whose slope is determined by the surface reflectivity. We also show that the atmospheric effects on C_T are relatively small at UV wavelengths longer than 310 nm. For these conditions the knowledge of C_T at one longer wavelength (e.g., 380 nm) and total ozone would be enough to determine C_T at shorter wavelengths with a high degree of accuracy (at least up to 310 nm, where absorption by tropospheric ozone is small).

2. At nonabsorbing UV wavelengths (e.g., 380 nm), C_T can be approximated from satellite reflectance measurements. Two methods are compared for the satellite estimation of C_T : the Lambert equivalent reflectivity (LER) method and the other based on radiative transfer calculations for a homogeneous (plane parallel) cloud embedded into molecular atmosphere with ozone absorption. Radiative transfer calculations show that the effects of cloud anisotropic reflectance from non-Lambertian surfaces are reduced in the plane perpendicular to the solar-principal plane. This is the geometry appropriate for the near-noon radiance measurements obtained from the TOMS satellite instrument. The plane-parallel cloud method predicts larger cloud transmittances than the LER method at 380 nm and for small solar zenith angles and accounts for the

C_T spectral dependence. Both effects result in higher C_T estimates at near UV wavelengths.

3. The satellite-derived C_T from the NASA Total Ozone Mapping Spectrometer (TOMS) is compared with ground-based C_T estimations from Canadian network of Brewer spectrometers for the period 1989–1998. For snow-free conditions the satellite-derived C_T at 324 nm agreed reasonably well with station data with a correlation coefficient of ~ 0.9 and a standard deviation of ~ 0.1 . The key source of uncertainty is the different size of the TOMS (~ 100 km) and the ground instrument (a few kilometers) field of view. As expected, the standard deviation of weekly (~ 0.06) and monthly (~ 0.04) C_T comparison averages was substantially smaller than for daily values.

4. When C_T values are averaged in solar zenith angle bins, it has been shown that the plane-parallel cloud method produces, on average, 7% higher C_T estimates than the Brewer C_T . Surprisingly, the simpler LER method agrees a bit better with ground data at low SZA than the more sophisticated plane-parallel cloud method. One possible explanation for this result is that at low SZA the real clouds, on aggregate, behave more like a Lambertian reflector at TOMS-viewing geometry than a plane-parallel cloud. The discrepancy at large SZA is currently not understood. One should conduct Monte Carlo studies to see if broken cloud models can resolve this discrepancy. More comparisons with ground-based C_T measurements at different locations are needed.

5. For snow-free conditions the running averages (10 days or more) of the spectral UV surface irradiances and daily doses can be inferred from the TOMS data (with possible systematic bias $\sim 20\%$ relative to ground-based instruments with their own biases). This is possible because most of the cloud high temporal/spatial variability can be treated as random process,

therefore this variability does not usually produce statistically significant biases after double averaging (spatial averaging over TOMS 100 km footprint and an additional time averaging over a period of 10 days or more). Thus the accuracy of the weekly to monthly TOMS UV products for snow-free conditions is sufficient for most biological applications.

6. The TOMS algorithm can properly account for conservatively scattering clouds and the presence of snow/ice if the reflectivity of the snow/ice is known from outside data. It is now possible to derive the regional snow-albedo climatology from ground-based measurements combined with satellite reflectivity data (examples are given for Brewer locations). However, the regional snow albedo varies on a daily basis, and using any kind of climatology (either satellite or ground based) will result in additional error in the satellite estimated C_T . Even if the snow albedo is known accurately, the C_T estimate becomes increasingly noisy over a highly reflecting surface. Thus the correlation between TOMS and Brewer C_T estimates becomes progressively worse with increasing average regional albedo associated with snow conditions. Currently, for sites with high surface albedo during winter months, TOMS can only estimate the average monthly irradiance with almost no correlation on a daily basis. This can be improved by developing regional snow albedo climatology, which should also be time dependent. For estimation of UV irradiance dosage, averaging cloud transmittance over at least a week should minimize errors caused by fresh-snow conditions compared to the true weekly dosage.

7. The effects of absorbing aerosols mixed with clouds on satellite C_T estimates were discussed. The polluted clouds transmit less radiation to the ground than conservative clouds for the same satellite reflectance and also modify the spectral dependence of C_T . Both effects effectively reduce the C_T compared to estimates assuming conservative cloud scattering. The error increases if clouds are over a snow surface. For a high reflecting surface (regional albedo >0.5), the satellite-measured reflectance becomes insensitive to cloud optical thickness and C_T cannot be estimated. The absorbing aerosols mixed with clouds also tend to flatten the spectral dependence of C_T . Better understanding of the C_T spectral dependence at UV-A wavelengths is required for determining limitations of the satellite UV measurements. Ground-based instruments simultaneously measuring global irradiance at least at two different wavelengths in the UV-A region can help achieve this result.

Appendix A: Enhanced Cloud Transmittance Over Snow

A homogeneous cloud layer reflects a greater percentage of the incident radiation when illuminated by diffuse source than it does for nearly normally incident solar irradiance (Figure 1). One important consequence is the theoretical possibility of enhanced cloud transmittance ($C_T > 1$) over a bright surface, when the top of the cloud is illuminated by direct Sun beam, while the bottom of the cloud is illuminated by diffuse radiation reflected from the surface. Considering a simple model of a homogeneous cloud layer above a Lambertian reflecting surface C_T can be expressed as a solution of the Stokes problem (see (2)):

$$C_T = C_{T0} = \frac{1 - R_C}{1 - R_S R_C^{\text{Diffuse}}} \quad (\text{A1})$$

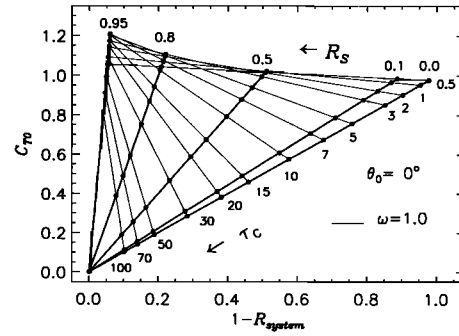


Figure A1. Relationship between C_{T0} and R_{System} for conservative scattering and overhead Sun. For a bright surface ($R_S > 0.5$), C_T first increases with increase in τ_C ($C_T > 1$) and then decreases with further increase in τ_C . Because of energy conservation the increase in C_T results in decrease in the reflectance of the system $R_{\text{System}} < R_S$. For enhanced transmittance atmospheric scattering decreases C_T at both UV-A and UV-B wavelengths.

The enhanced transmittance ($C_T > 1$) is possible if

$$R_C < R_S R_C^{\text{Diffuse}}, \quad (\text{A2})$$

where R_S is the surface reflectivity (albedo), R_C and R_C^{Diffuse} are hemispherical albedos of the cloud layer illuminated by a direct and diffuse source for zero surface reflectivity (see Table 1). For a homogeneous cloud layer, R_C and R_C^{Diffuse} can be obtained using a two stream analytical approximation for conservative scattering [Coakley and Chylek, 1975] (see Figure 1):

$$R_C = \frac{\tau_C^*}{\tau_C^* + 2\mu_0}, \quad \tau_C^* = (1 - g)\tau_C, \quad \mu_0 = \cos(\theta_0), \quad (\text{A3})$$

where g is the asymmetry factor (mean cosine) of the cloud phase function. We note that for a fixed τ_C , R_C is minimal for overhead Sun and increases with increase in solar zenith angle (see Figure 1). Therefore cloud layer reflects more radiation when illuminated by diffuse source than it does for nearly normally incident solar irradiance: $R_C^{\text{Diffuse}} > R_C$ ($\mu_0 \sim 1$). Using (A3) for R_C , one can also obtain the approximate solution for hemispherical albedo when the cloud is illuminated by diffuse source, R_C^{Diffuse} :

$$R_C^{\text{Diffuse}} = 2 \int R_C(\mu_0) \mu_0 d\mu_0 = \tau_C^* \left[1 - \frac{1}{2} \tau_C^* \ln \left(1 + \frac{2}{\tau_C^*} \right) \right]; \quad (\text{A4})$$

combining (A2), (A3), and (A4), we obtain the necessary condition for enhanced cloud transmittance:

$$\frac{\tau_C^*}{\tau_C^* + 2\mu_0} < R_S R_C^{\text{Diffuse}}. \quad (\text{A5})$$

From this equation, one can see that a combination of low solar-zenith angle ($\mu_0 \sim 1$) and high surface albedo is required for enhanced cloud transmittance ($C_T > 1$). In this regime the cloud layer becomes more transparent from above (direct solar radiation) than from below (diffuse illumination by the snow surface). Therefore photons are “trapped” between the surface and the cloud bottom (“cavity” effect). The cloud optical thickness can vary in a wide range (e.g., $\tau_C = 1-50$). We note that $C_T > 1$ regime does not violate energy conservation. Figure A1 shows the relationship between C_T and R_{System} for conservative scattering ($\omega = 1.0$), overhead Sun and different

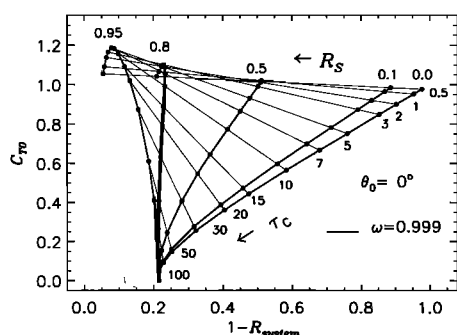


Figure A2. Same as Figure A1 except the single-scattering albedo of the cloud is 0.999.

combinations of R_s and τ_c . The enhanced transmittance ($C_T > 1$) does not occur for low Sun, because $R_C > R_C^{\text{Diffuse}}$ (see the case with $\mu_0 = 0.5$ in Figures 1 and 2). Also, optically thick clouds ($\tau_c > 40$) eventually reduce C_T to less than a unity even for extremely bright surface and high Sun (see Figure A1). The enhanced cloud transmittance is also possible for nonconservative cloud scattering (Figure A2) and for the cloud layer embedded into molecular atmosphere (see Figure 4 for $R_s = 0.8$ and $\theta_0 = 0^\circ$).

Acknowledgments. We thank the members of the TOMS team at Goddard Space Flight Center for producing the data sets upon which this work is based. In addition, we wish to thank Edward Celarier for preparation of the UV data set from the measured TOMS radiances, Alexander Marshak, as well as contributions from Tom Eck, Omar Torres, Christina Hsu, Alexander Vasilkov, and Gordon Labow. We also wish to thank the reviewers for valuable suggestions. The work was supported by the NASA TOMS program.

References

- Ahmad, Z., and R. Fraser, An iterative radiative transfer code for ocean-atmosphere systems, *J. Atmos. Sci.*, **39**, 656–665, 1982.
- Bais, A. F., S. Kazadzis, D. Balis, C. Zerefos, and M. Blumthaler, Correcting global solar ultraviolet spectra recorded by a Brewer spectroradiometer for its angular response error, *Appl. Opt.*, **37**, 6339–6344, 1998.
- Bohren, C. F., and B. R. Barkstorm, Theory of the optical properties of snow, *J. Geophys. Res.*, **79**, 4527–4535, 1974.
- Brühl, C., and P. J. Crutzen, On the disproportional role of tropospheric ozone as a filter against UV-B radiation, *Geophys. Res. Lett.*, **16**, 703–706, 1989.
- Chandrasekhar, S., *Radiative Transfer*, 393 pp., Oxford Univ. Press, New York, 1960.
- Chubarova, N. B., Ultraviolet radiation under broken cloud conditions as inferred from many-year ground-based observations, *Izv. Atmos. Oceanic Phys.*, **34**, 131–135, 1998.
- Chylek, P., et al., Black carbon and absorption of solar radiation by clouds, *J. Geophys. Res.*, **101**, 23,365–23,371, 1996.
- Coakley, J. A., Jr., and P. Chylek, The two-stream approximation in radiative transfer: Including the angle of the incident radiation, *J. Atmos. Sci.*, **32**, 409–418, 1975.
- Dave, J. V., Effect of aerosols on the estimation of total ozone in an atmospheric column from the measurements of its ultraviolet radiance, *J. Atmos. Sci.*, **35**, 899–911, 1978.
- Davies, R., Increased transmission of ultraviolet radiation to the surface due to stratospheric scattering, *J. Geophys. Res.*, **98**, 7251–7253, 1993.
- Deirmendjian, D., *Electromagnetic Scattering on Spherical Polydispersions*, 290 pp., Elsevier Sci., New York, 1969.
- Dickerson, R. R., S. Kondragunta, G. Stenchikov, K. L. Civerolo, B. G. Doddridge, and B. N. Holben, The impact of aerosols on solar ultraviolet radiation and photochemical smog, *Science*, **278**, 827–830, 1997.
- Dye, D. G., and R. Shibasaki, Intercomparison of Global PAR data sets, *Geophys. Res. Lett.*, **22**, 2013–2016, 1995.
- Eck, T. F., and G. Dye, Satellite estimation of incident photosynthetically active radiation using ultraviolet reflectance, *Remote Sens. Environ.*, **38**, 135–146, 1991.
- Eck, T. F., P. K. Bhartia, P. H. Hwang, and L. L. Stowe, Reflectivity of Earth's surface and clouds in ultraviolet from satellite observations, *J. Geophys. Res.*, **92**, 4287–4296, 1987.
- Eck, T. F., P. K. Bhartia, and J. B. Kerr, Satellite Estimation of spectral UV-B irradiance using TOMS derived ozone and reflectivity, *Geophys. Res. Lett.*, **22**, 611–614, 1995.
- Erlick, C. J., and J. E. Frederick, Effects of aerosols on the wavelength dependence of atmospheric transmission in the ultraviolet and visible, **2**, Continental and urban aerosols in clear skies, *J. Geophys. Res.*, **103**, 23,275–23,285, 1998.
- Erlick, C., J. E. Frederick, V. K. Saxena, and B. N. Wenny, Atmospheric transmission in the ultraviolet and visible: Aerosols in cloudy atmospheres, *J. Geophys. Res.*, **103**, 31,541–31,556, 1998.
- Fioletov, V. E., and W. F. J. Evans, The influence of ozone and other factors on surface radiation, in *Ozone Science: A Canadian Perspective on the Changing Ozone Layer*, edited by D. I. Wardle, J. B. Kerr, C. T. McElroy, and D. R. Francis, *CARD 97-3, AES Rep.*, pp. 73–90, Atmos. Environ. Ser., Downsview, Ontario, Canada, 1997.
- Fioletov, V. E., J. B. Kerr, and D. I. Wardle, The relationship between total ozone and spectral UV irradiance from Brewer spectrophotometer observations and its use for derivation of total ozone from UV measurements, *Geophys. Res. Lett.*, **24**, 2997–3000, 1997.
- Frederick, J. E., and C. Erlick, The attenuation of sunlight by high latitude clouds: Spectral dependence and its physical mechanisms, *J. Atmos. Sci.*, **54**, 2813–2819, 1997.
- Frederick, J. E., and D. Lubin, The budget of biologically active ultraviolet radiation in the Earth-atmosphere system, *J. Geophys. Res.*, **93**, 3825–3832, 1988.
- Grenfell, T. C., S. G. Warren, and P. C. Mullen, Reflection of solar radiation by the Antarctic snow surface at ultraviolet, visible, and near-infrared wavelengths, *J. Geophys. Res.*, **99**, 18,669–18,684, 1994.
- Herman, J. R., and E. Celarier, Earth Surface Reflectivity Climatology at 340 nm to 380 nm from TOMS Data, *J. Geophys. Res.*, **102**, 28,003–28,011, 1997.
- Herman, J. R., P. K. Bhartia, J. Ziemke, Z. Ahmad, and D. Larko, UV-B increases (1979–1992) from decreases in total ozone, *Geophys. Res. Lett.*, **23**, 2117–2120, 1996.
- Herman, J. R., N. Krotkov, E. Celarier, D. Larko, and G. Labow, Distribution of UV radiation at the Earth's surface from TOMS-measured UV-backscattered radiances, *J. Geophys. Res.*, **104**, 12,059–12,076, 1999.
- Hsu, C. N., R. D. McPeters, C. J. Seftor, and A. M. Thompson, Effect of an improved cloud climatology on the total ozone mapping spectrometer total ozone retrieval, *J. Geophys. Res.*, **102**, 4247–4255, 1997.
- Jacobson, M. Z., Isolating nitrated and aromatic aerosols and nitrated aromatic gases as sources of ultraviolet light absorption, *J. Geophys. Res.*, **104**, 3527–3542, 1999.
- Joiner, J., P. K. Bhartia, R. C. Cebula, E. Hilsenrath, R. D. McPeters, and H. Park, Rotational Raman scattering (Ring effect) in satellite backscatter ultraviolet measurements, *Appl. Opt.*, **34**, 4513–4525, 1995.
- Kalliskota, S., J. Kaurola, P. Taalas, J. R. Herman, E. A. Celarier, and N. A. Krotkov, Comparison of daily UV doses estimated from Nimbus-7/TOMS measurements and ground-based spectroradiometric data, *J. Geophys. Res.*, **105**, 5059–5067, 2000.
- King, M. L., L. F. Radke, and P. V. Hobbs, Determination of the spectral absorption of solar radiation by marine stratocumulus clouds from airborne measurements within clouds, *J. Atmos. Sci.*, **47**, 894–907, 1990.
- Krotkov, N. A., P. K. Bhartia, J. Herman, E. Celarier, and T. Eck, Estimates of spectral UVB irradiance from the TOMS instrument: Effects of clouds and aerosols, in *IRS'96: Current Problems in Atmospheric Radiation*, edited by W. L. Smith and Knut Stamnes, pp. 873–876, A. Deepak, Hampton, Va., 1997.
- Krotkov, N. A., P. K. Bhartia, J. R. Herman, V. Fioletov, and J. Kerr, Satellite estimation of spectral surface UV irradiance in the presence of tropospheric aerosols, **1**, Cloud-free case, *J. Geophys. Res.*, **103**, 8779–8793, 1998.
- Kylling, A., A. F. Bais, M. Blumthaler, J. Schreder, C. S. Zerefos, and E. Kosmidis, Effect of aerosols on solar UV irradiance during the

- photochemical activity and solar ultraviolet radiation campaign, *J. Geophys. Res.*, **103**, 26,051–26,060, 1998.
- Kylling, A., T. Persen, B. Mayer, and T. Svenoe, Determination of an effective spectral surface albedo from ground-based global and direct UV irradiance measurements, *J. Geophys. Res.*, **105**, 4949–4959, 2000.
- Lenoble, J., Modeling of the influence of snow reflectance on ultraviolet irradiance for cloudless sky, *Appl. Opt.*, **37**, 2441–2447, 1998.
- Li, Z., P. Wang, and J. Cihlar, A simple and efficient method for retrieving surface UV radiation dose rate from satellite, *J. Geophys. Res.*, **105**, 5027–5036, 2000.
- Liu, S. C., S. A. McKeen, and S. Madronich, Effect of anthropogenic aerosols on biologically active ultraviolet radiation, *Geophys. Res. Lett.*, **18**, 2265–2268, 1991.
- Lubin, D., and E. H. Jensen, Effects of clouds and stratospheric ozone depletion on ultraviolet radiation trends, *Nature*, **377**, 710–713, 1995.
- Lubin, D., P. Ricchiazzi, C. Gautier, and R. H. Whritner, A method for mapping Antarctic surface ultraviolet radiation using multispectral satellite imagery, in *Ultraviolet Radiation in Antarctica: Measurements and Biological Effects*, *Antarct. Res. Ser.*, vol. 62, edited by C. S. Weiler, and P. A. Penhale, pp. 53–82, AGU, Washington, D. C., 1994.
- Lubin, D., E. H. Jensen, and H. P. Gies, Global surface ultraviolet radiation climatology from TOMS and ERBE data, *J. Geophys. Res.*, **103**, 26,061–26,091, 1998.
- Madronich, S., Implications of recent total ozone measurements for biologically active ultraviolet radiation on reaching the Earth's surface, *Geophys. Res. Lett.*, **19**, 37–40, 1992.
- Madronich, S., The atmosphere and UV-B radiation at ground level, in *Environmental UV Photobiology*, edited by A. R. Young et al., pp. 1–39, Plenum, New York, 1993.
- Matthijsen, J., H. Slaper, H. A. G. M. Reinen, and G. J. M. Velders, Reduction of solar UV by clouds: A remote sensing approach compared with ground-based measurements, *J. Geophys. Res.*, **105**, 5069–5080, 2000.
- Mayer, B., G. Seckmeyer, and A. Kylling, Systematic long-term comparison of spectral UV measurements and UVSPEC modeling results, *J. Geophys. Res.*, **102**, 8755–8767, 1997.
- Mayer, B., C. A. Fischer, and S. Madronich, Estimation of surface actinic flux from satellite (TOMS) ozone and cloud reflectivity measurements, *Geophys. Res. Lett.*, **25**, 4321–4324, 1998a.
- Mayer, B., A. Kylling, S. Madronich, and G. Seckmeyer, Enhanced absorption of UV irradiance due to multiple scattering in clouds: Experimental evidence and theoretical explanation, *J. Geophys. Res.*, **103**, 31,241–31,254, 1998b.
- McCormick, P. G., and H. Suehrcke, Cloud-reflected radiation, *Nature*, **345**, 773, 1990.
- McKenzie, R. L., M. Kotkamp, and W. Ireland, Upwelling UV spectral irradiances and surface albedo measurements at Lauder, New Zealand, *Geophys. Res. Lett.*, **23**, 1757–1760, 1996.
- McPeters, R. D., et al., Nimbus-7 Total Ozone Mapping Spectrometer (TOMS) data products user's guide, *NASA Ref. Publ. 1384*, 1996.
- Meerkötter, R., B. Wissinger, and G. Seckmeyer, Surface UV from ERS-2/GOME and NOAA/AVHRR data: A case study, *Geophys. Res. Lett.*, **24**, 1939–1942, 1997.
- Melnikova, I. N., and V. V. Mikhailov, Spectral scattering and absorption coefficients in strati derived from aircraft measurements, *J. Atmos. Sci.*, **51**, 925–931, 1994.
- Mims, F. M., III, and J. E. Frederick, Cumulus clouds and UV-B, *Nature*, **371**, 291, 1994.
- Nack, M. L., and A. E. S. Green, Influence of clouds, haze and smog on the middle ultraviolet reaching the ground, *Appl. Opt.*, **13**(N10), 2405–2415, 1974.
- Peeters, P., J. F. Muller, P. C. Simon, E. Celarier, and J. R. Herman, Estimation of UV flux at the Earth's surface from GOME data, *ESA Earth Obs.*, **58**, 39–40, 1998.
- Rossow, W. B., and R. A. Schiffer, ISCCP cloud data products, *Bull. Am. Meteorol. Soc.*, **72**, 2–20, 1991.
- Rublev, A. N., A. N. Trotsenko, N. E. Chubarova, O. M. Isakova, I. V. Georgidze, T. V. Kondranin, P. Y. Romanov, The use of satellite data for determination of downward solar radiation fluxes at cloudy conditions and their comparison with ground-based measurements, in *IRS'96: Current Problems in Atmospheric Radiation*, edited by W. Smith and K. Stamnes, pp. 488–491, A. Deepak, Hampton, Va., 1997.
- Sabziparvar, A. A., P. M. de F. Forster, and K. P. Shine, Changes in ultraviolet radiation due to stratospheric and tropospheric ozone changes since preindustrial times, *J. Geophys. Res.*, **103**, 26,107–26,113, 1998.
- Schwander, H., P. Koepke, and A. Ruggaber, Uncertainties in modeled UV irradiance due to limited accuracy and availability of input data, *J. Geophys. Res.*, **102**, 9419–9429, 1997.
- Schwander, H., B. Mayer, A. Ruggaber, A. Albold, G. Seckmeyer, and P. Koepke, Method to determine snow albedo values in the ultraviolet for radiative transfer modeling, *Appl. Opt.*, **38**, 3869–3875, 1999.
- Seckmeyer, G., R. Erb, and A. Albold, Transmittance of a cloud is wavelength dependent in the UV range, *Geophys. Res. Lett.*, **23**(19), 2625–2628, 1996.
- Soulen, P. F., and J. F. Frederick, Estimating biologically active UV irradiance from satellite radiance measurements: A sensitivity study, *J. Geophys. Res.*, **104**, 4117–4126, 1999.
- Stamnes, K., S. C. Tsay, W. Wiscombe, and K. Jayaweera, Numerically stable algorithm for discrete-ordinate-method radiative transfer in multiple scattering and emitting layered media, *Appl. Opt.*, **27**, 2502–2509, 1988.
- Suttles, J. T., R. N. Green, G. L. Smith, B. A. Wielicki, I. J. Walker, V. R. Taylor, and L. L. Stowe, Angular radiation models for the Earth-atmosphere system, vol. 1, Shortwave radiation, *NASA Ref. Publ. RP-1184*, 159 pp., 1989.
- Taylor, V. R., and L. L. Stowe, Reflectance characteristics of uniform earth and cloud surfaces derived from Nimbus-7 ERB, *J. Geophys. Res.*, **89**, 4897–4996, 1984.
- Torres, O., P. K. Bhartia, J. R. Herman, and Z. Ahmad, Derivation of aerosol properties from satellite measurements of backscattered ultraviolet radiation, theoretical basis, *J. Geophys. Res.*, **103**, 17099–17110, 1998.
- Twomey, S., The effect of cloud scattering on the absorption of solar radiation by atmospheric dust, *J. Atmos. Sci.*, **29**, 1156–1159, 1972.
- Twomey, S., and C. F. Bohren, Simple approximations for calculations of absorption in clouds, *J. Atmos. Sci.*, **37**, 2086–2094, 1980.
- Twohy, C. H., A. D. Clarke, S. G. Warren, L. F. Radke, and R. J. Charlson, Light-absorbing material extracted from cloud droplets and its effect on cloud albedo, *J. Geophys. Res.*, **94**, 8623–8631, 1989.
- Verdebot, J. A., Method to generate surface UV radiation maps over Europe using GOME, Meteosat, and ancillary geophysical data, *J. Geophys. Res.*, **105**, 5049–5058, 2000.
- Vogelmann, A. M., T. P. Ackerman, and R. P. Turco, Enhancements in biologically effective ultraviolet radiation following volcanic eruptions, *Nature*, **359**, 47–49, 1992.
- Weih, P., and A. R. Webb, Accuracy of spectral UV model calculations, 2, Comparison of UV calculations with measurements, *J. Geophys. Res.*, **102**, 1551–1560, 1997.
- Wendisch, M., and A. Keil, Discrepancies between measured and modeled solar and UV radiation within polluted boundary layer clouds, *J. Geophys. Res.*, **104**, 27,373–27,385, 1999.
- World Meteorological Organization (WMO), Scientific Assessment of Ozone Depletion: 1998, Global Ozone Res. and Monit. Proj., *WMO Rep. 44*, Geneva, Switzerland, 1999.
- Z. Ahmad, Science and Data Systems, 16509 Copperstrip Lane, Silver Spring, MD 20906.
- P. K. Bhartia and J. R. Herman, Laboratory for Atmospheres, NASA Goddard Space Flight Center, Code 91b, Greenbelt, MD 20771.
- V. Fioletov, Meteorological Service of Canada, Downsview, Ontario, Canada M3H 5T4.
- N. A. Krotkov, NASA Goddard Space Flight Center, Code 916, Bldg. 33, Room E411, Greenbelt, MD 20771. (krotkov@chescat.gsfc.nasa.gov)

(Received May 4, 2000; revised October 23, 2000; accepted October 26, 2000.)